Received: 3 July 2023 | Revised: 29 August 2023 | Accepted: 2 September 2023

DOI: 10.1002/ece2.4

REVIEW

EcoEnergy WILEY

Design strategies of ruthenium-based materials toward alkaline hydrogen evolution reaction

Liqiang Hou[1] | **Haeseong Jang**[2] | **Xiumin Gu**[1] | **Xuemei Cui**[1] | **Jiachen Tang**[1] | **Jaephil Cho**[3] | **Xien Liu**[1]

[1]State Key Laboratory Based of Eco-Chemical Engineering, College of Chemical Engineering, Qingdao University of Science and Technology, Qingdao, China

[2]Department of Advanced Materials Engineering, Chung-Ang University, Seoul, South Korea

[3]Department of Energy Engineering, Department of Energy and Chemical Engineering, Ulsan National Institute of Science and Technology (UNIST), Ulsan, South Korea

Correspondence
Jaephil Cho and Xien Liu.
Email: jpcho@unist.ac.kr and liuxien@qust.edu.cn

Funding information
Natural Science Foundation of Shandong Province of China, Grant/Award Number: ZR2022QB100; Science Foundation of Qingdao University of Science and Technology, Grant/Award Number: 12030430010936

Abstract

Hydrogen produced from electrocatalytic water splitting means is deemed to be a promising route to construct a low-carbon, eco-friendly, and high-efficiency modern energy system. The design and construction of highly active catalysts with affordable prices toward alkaline hydrogen evolution reaction (HER) are effective in accelerating the overall water-splitting process. So far, ruthenium (Ru) based catalysts deliver comparable or even superior catalytic performance relative to the platinum (Pt)/C benchmark. Combined with their price advantage, Ru-based catalysts are undoubtedly considered as one of the perfect alternatives of Pt toward the alkaline HER. Extensive efforts have been made to reasonably synthesize Ru-related materials, but a careful insight into material engineering strategies and induced effects remain in its infancy. In this review, recent progress on the material engineering strategies for improving the catalytic activity of Ru-related catalysts, including electronic regulation, geometric modulation, local structure alteration, self-optimization strategies, and the induced structure–activity relationship are comprehensively summarized. Furthermore, the challenges and perspectives on future studies of Ru-related electrocatalysts for the alkaline HER are also proposed.

KEYWORDS
alkaline condition, challenges and perspectives, hydrogen evolution reaction, modification strategies, ruthenium-based materials

1 | INTRODUCTION

Hydrogen is a promising secondhand energy with bountiful sources, environmentally friendly, and zero-carbon. It can help renewable energy to be absorbed on a large scale, and realize massive peak adjustment of the power grid and cross-seasonal and cross-regional energy store.[1–4] The production of hydrogen through a low-cost and highly efficient means is a decisive issue and has long been explored. Compared to industrial steam reforming with low-purity hydrogen, electrochemical water splitting in alkaline conditions provides an effective and promising route to produce hydrogen with high purity.[5–7] More importantly, such technology can be driven

by renewable energy sources. Nevertheless, the reaction kinetics of cathodic hydrogen evolution reaction (HER) in alkaline conditions is relatively sluggish and urgently needs highly active HER catalysts to accelerate the whole process.[8–11] Moreover, the alkaline HER also plays a determining role in the energy-intensive chlor-alkali technique.[12–14] Thus, the design and construction of significantly active catalysts toward the alkaline HER is greatly significant for future energy saving and pollution reduction.

The sluggish reaction kinetics of the alkaline HER are caused by the indispensable H_2O cleaving step, which produces the hydrogen protons required for succedent reaction steps.[15–17] As illustrated in Figure 1, there are two steps for the alkaline HER process including H_2O dissociation and H_2 generation.[18,19] Firstly, the water molecule is dissociated into a hydroxyl ion and an adsorbed hydrogen proton on the active site (Volmer step). Afterward, two adsorbed hydrogen protons combine to produce a hydrogen molecule (Tafel step), or the adsorbed hydrogen proton combines with a water molecule by interaction to produce a hydrogen molecule (Heyrovsky step). In a word, the total reaction steps of HER in alkaline conditions are shown in the following equations.

$$H_2O + e^- \rightarrow H^* + OH^- \text{ (Volmer)}$$

$$2H^* \rightarrow H_2 \text{ (Tafel) or } H_2O + e^- + H^* \rightarrow H_2 + OH^- \text{ (Heyrovsky)}$$

Of note, the catalysts of the alkaline HER should ensure both steps with fast reaction kinetics, leading to the design of advanced catalysts with high activity difficulties.[20]

Noble metal platinum (Pt) is deemed to be the "Holy Grail" toward the electrocatalytic reactions related to hydrogen/oxygen.[21–24] Nevertheless, the large-scale use of Pt-based catalysts is mainly subjected to its high cost. Lately, Pt-group ruthenium (Ru) has been widely explored to act as one of the hopeful alternatives of Pt, which is attributed to its comparatively low price.[25,26] Until now, extensive efforts have been made to elaborately synthesize greatly active Ru-based electrocatalysts for the alkaline HER, and many of them display considerable and even superior performance than the commercial Pt/C benchmark.[27,28] Although some excellent related reviews have been published,[29,30] the rational design strategies to construct Ru-based materials, coupled with their structure–activity relationship toward the alkaline HER, are lacking and desired. This review mainly summarizes the material engineering strategies for improving the catalytic performance of Ru-related catalysts, including electronic regulation, geometric modulation, local structure alteration, and self-optimization, and analyzes in detail the induced structure–activity relationship for the alkaline HER. Finally, the challenges and opportunities of designing greatly active Ru-based materials toward the alkaline HER are proposed.

2 | MATERIAL ENGINEERING ON Ru-BASED ELECTROCATALYSTS

The material engineering on Ru-based electrocatalysts for the alkaline HER can efficaciously regulate their electronic properties, thus inducing the regulation of adsorption energy for the reaction intermediates and the decrease in the reaction energy barrier of the decision step. Hence, developing appropriate engineering strategies to enhance the overall performances of Ru-related catalysts is effective and desired. This part will summarize the material engineering strategies on Ru-related catalysts toward the alkaline HER as illustrated in Figure 2 and Table 1.

2.1 | Electronic regulation

The electronic structure of Ru-related electrocatalysts is of the utmost importance to their catalytic activity for the

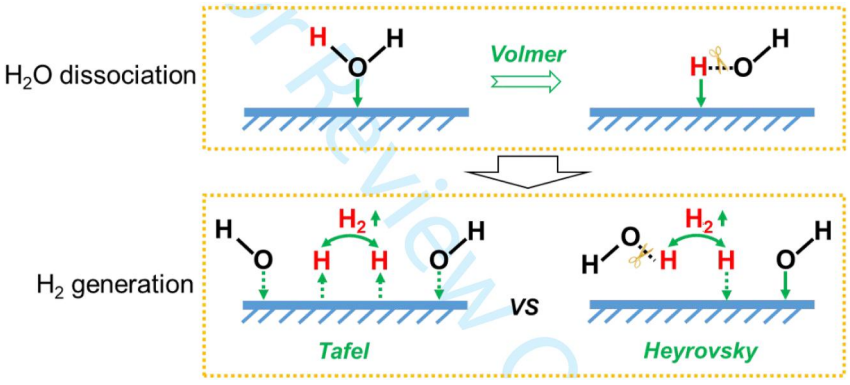

FIGURE 1 A scheme illustrating hydrogen evolution reaction mechanism in alkaline conditions.

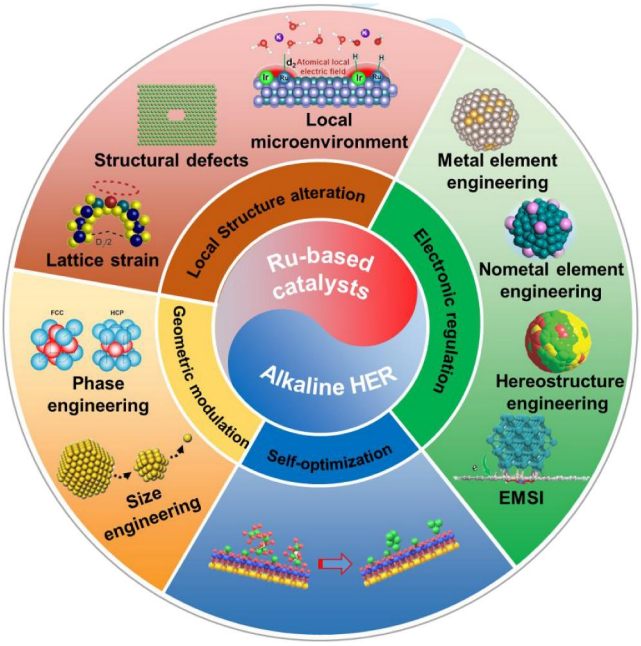

FIGURE 2 Visualized overview of strategies to enhance the catalytic performance of Ru-based catalysts toward the alkaline HER. HER, hydrogen evolution reaction; Ru, ruthenium.

alkaline HER, which is closely relevant to the interaction force between reaction intermediates and active sites.[71,72] In general, electronic regulation includes metal element engineering, nonmetal element engineering, heterostructure engineering, and electronic metal–support interaction (EMSI).

2.1.1 | Metal element engineering

Alloying with foreign metal atoms can greatly enhance the intrinsic catalytic properties of the Ru metal host, which is attributed to the electronic regulation effect of other metals with different atomic radii and electronegativity.[31–33,73] In addition, the introduced foreign metal atoms may serve as extra catalytic active sites to collectively improve the alkaline HER activity. For example, Chen et al. prepared the RuAu single-atom alloy (RuAu SAA) through the liquid laser ablation method (Figure 3A).[31] It is to be noted that, the Au atoms occupied the locations of Ru atoms and were atomically dispersed in the Ru host (Figure 3B). Thus, the RuAu SAA displayed a superior alkaline HER activity (24 mV@10 mA cm^{-2}), lower than that of Pt/C (46 mV). Combining experimental and theoretical data indicated that the introduction of Au into the Ru host not only regulated the electronic properties of Ru with the electron transfer from Ru to Au but also induced relay catalysis with Ru atoms as H_2O splitting sites and Au atoms as H_2 formation sites (Figure 3C). Mu et al. prepared defect-rich $RuRh_2$ bimetallene nanorings by hydrothermal reaction (Figure 3D,E).[32] $RuRh_2$ bimetallene presented a lower overpotential of 24 mV at 10 mA cm^{-2} for the alkaline HER relative to Pt (32 mV). They found that the electronic properties of $RuRh_2$ bimetallene were effectively adjusted by the synergistic effect, including the alloying effect, the strain effect from the $RuRh_2$, and the quantum size effect induced by its unique nanostructure, which highly promoted the optimization of the hydrogen adsorption energy of H intermediate and dissociation energy of absorbed water (Figure 3F).

Other than alloying with noble metals, the incorporation of abundant transition metals can not only improve the activity of Ru by regulating its electronic properties but also greatly lower the consumption of noble Ru metal.[33–35] Liu et al. designed a scalable and general synthetic strategy for the preparation of bimetallic RuM/CQDs (RuNi, RuMn, RuCu) using carbon quantum dots as both the carbon and nitrogen sources (Figure 3G).[33] Taking RuNi/CQDs as an example, physical structure characterizations indicated the formation of RuNi alloy and uniformly doped Ni, which had a low Ru content of 1.42 wt% (Figure 3H). Excitingly, the RuNi/CQDs delivered a low overpotential of 13 mV at a current density of 10 mA cm^{-2} toward the alkaline HER. Moreover, its mass activity was 24 times greater than that of the commercial Pt/C at 13 mV. Characterization analysis and theoretical calculation indicated that Ni doping in the Ru lattice led to a negatively charged Ru and significantly lowered the adsorption energy of H*, hence increasing the catalytic performance of RuNi/CQDs for the alkaline HER (Figure 3I). Note that the modification carbon matrix by metal doping can also further optimize the binding energy of active sites. Zhao et al. constructed a RuBi atomic alloy nanoparticle anchored on graphene with the dopant of single Bi atoms (RuBi SAA/Bi@OG) via a one-step pyrolysis strategy (Figure 3J,K).[34] XAS and XPS studies revealed the charge redistribution on the Ru was induced by the synergistic regulation from the introduction of single Bi atoms and neighboring Bi-O-C species, which could accelerate reaction kinetics for the alkaline HER. Consequently, the RuBi SAA/Bi@OG presented a smaller overpotential of 17.5 mV compared to Pt/C (37.8 mV) at 10 mA cm^{-2} in an alkaline electrolyte. Moreover, its mass activity was 72.2 times higher than that of the commercial Pt/C at 150 mV. Theoretical calculations indicated that the double atomic-tuned method induced the charge optimization of Ru nanoparticles, which promoted the optimization of H_2O dissociation and H_2 adsorption behavior on the Ru active sites (Figure 3L).

TABLE 1 Summary of representative Ru-based electrocatalysts toward the alkaline HER.

Material engineering strategies	Catalysts	Electrolyte	Overpotential (mV) at 10 mA cm^{-2}	Tafel slope (mV dec^{-1})	Overpotential (mV) of Pt/C at 10 mA cm^{-2}	References
Electronic regulation	RuAu SAA	1 M KOH	24	37	46	31
	$RuRh_2$ bimetallene	1 M KOH	24	31	32	32
	RuNi/CQDs	1 M KOH	13	40	-	33
	RuBi SAA/Bi@OG	1 M KOH	17.5	29.2	37.8	34
	RuCo ANSs	1 M KOH	10	20.6	-	35
	RuNi NSs	1 M KOH	15	28	54	36
	RuCu NSs	1 M KOH	20	15.3	60	37
	LaRuSi	1 M KOH	72	68	-	38
	FeCoNiMnRu HEA	1 M KOH	71/100 mA cm^{-2}	67.4	-	39
	P-Ru/C	1 M KOH	31	105	39	40
	P,Mo-Ru@PC	1 M KOH	21	21.7	33	27
	S-RuP@NPSC	1 M KOH	92	90.23	-	41
	2DPC-RuMo	1 M KOH	18	25	32	42
	Ru-Ru_2P	1 M KOH	18	30.2	37	43
	Ru_2P/WO_3@NPC	1 M KOH	15	18	23	44
	Ru/Ni/WC@NPC	1 M KOH	3	33.4	20	45
	Ru@GnP	1 M KOH	22	28	33	46
	Ru NCs/BNG	1 M KOH	14	28.9	26	47
	Ru/Co@OG	1 M KOH	13	22.8	31	48
	Ru-Fe_3O_4/C	1 M KOH	11	25	17	49
	Ru/r-TiO_2	1 M KOH	15	49	34	50
	Ru/P-TiO_2	1 M KOH	27	28.3	-	51
	Ru/HfO_2	1 M KOH	39	29	22	52
	$NiRu_{0.13}$-BDC	1 M KOH	34	32	-	53
	Ru@Ni-MOF	1 M KOH	22	40	46	54
Geometric modulation	Ru_{SA+NP}/DC	1 M KOH	18.8	35.8	32.2	55
	Ru-1.0	1 M KOH	13	25.3	38	56
	NCPO-Ru NCs	1 M KOH	11	29	27	57
	4H/fcc Ru NTs	1 M KOH	23	29.4	46	58
	Ru MNSs	1 M KOH	24	33.8	70	59
Local structure alteration	PdH_x@Ru	1 M KOH	30	30	46	60
	$CoRu_{0.5}$/CQDs	1 M KOH	18	38.5	30	61
	Ru/np-MoS_2	1 M KOH	30	31	-	62
	$Ru_{0.85}Zn_{0.15}O_{2-\delta}$	1 M KOH	14	29	32	63
	DR-Ru	1 M KOH	28.2	40.8	61.2	64
	Pyrite-type RuS_2	1 M KOH	78	50	-	65
	NA-Ru_3Ni	1 M KOH	54/100 mA cm^{-2}	28	88/100 mA cm^{-2}	66
	IrRu DSACs	1 M KOH	10	34	31	67

(Continues)

TABLE 1 (Continued)

Material engineering strategies	Catalysts	Electrolyte	Overpotential (mV) at 10 mA cm^{-2}	Tafel slope (mV dec^{-1})	Overpotential (mV) of Pt/C at 10 mA cm^{-2}	References
Self-optimization	Ru/NC	1 M KOH	25	29	24	68
	SRO single crystal	1 M KOH	18	22	17	69
	PtRu/mCNTs	1 M KOH	15	33.5	39	70

Abbreviations: CQDs, carbon quantum dots; HEA, high entropy alloys; HER, hydrogen evolution reaction; Ru, ruthenium; SAA, single-atom alloy; SRO, Sr_2RuO_4.

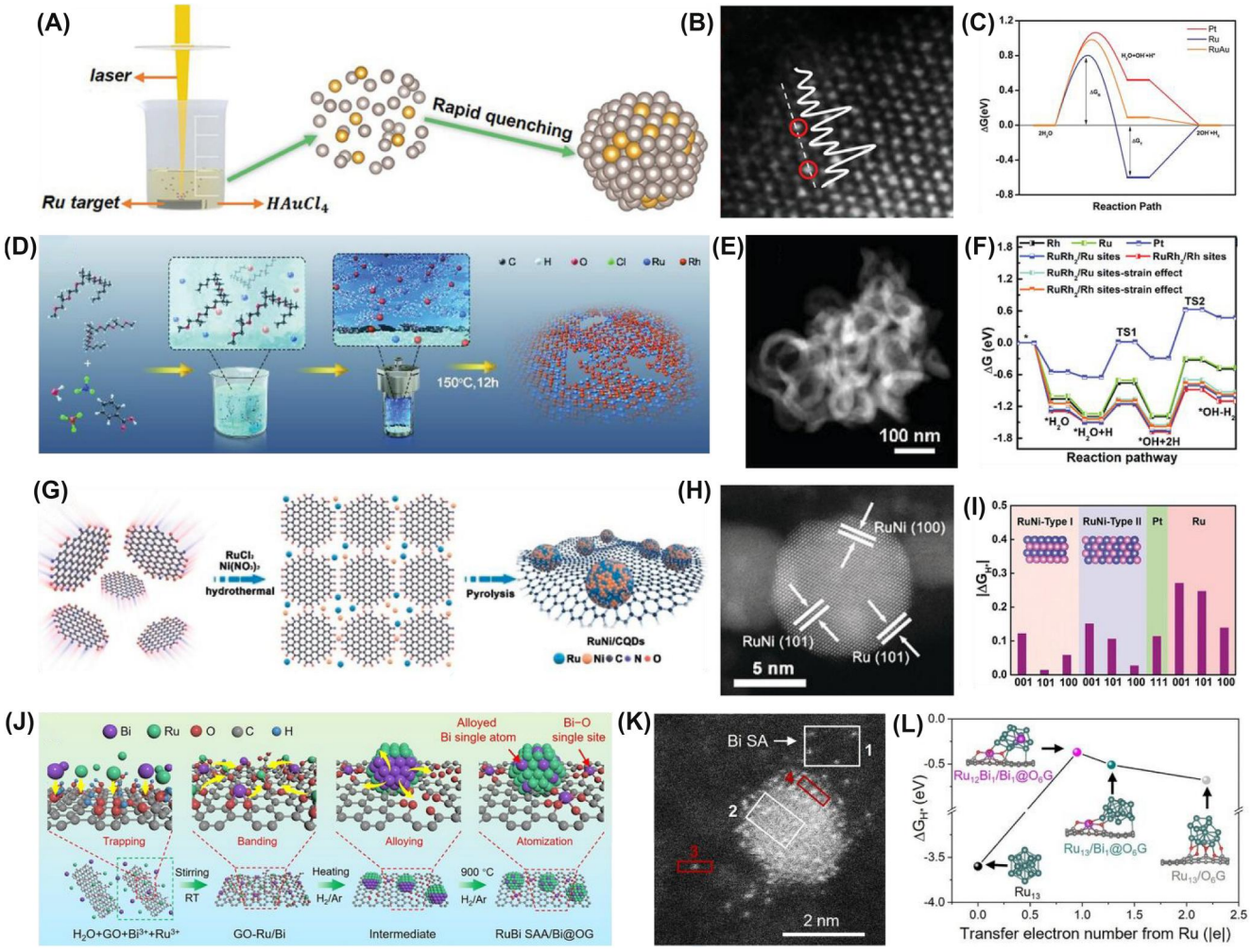

FIGURE 3 (A) The schematic setup of PLAL and the formation process of SAA nanoparticles. (B) Atomic-resolution HAADF-STEM image, Au atoms (marked by red circles) are uniformly distributed throughout the particle. (C) Thermodynamic and kinetic barriers for hydrogen evolution in three catalysts.[31] Copyright 2019 Wiley-VCH. (D) Schematic illustration of the synthetic process of the $RuRh_2$ bimetallene nanoring catalyst. (E) HAADF-STEM image of $RuRh_2$ nanorings. (F) Free energy diagrams for water dissociation potential on Rh top site, Ru top site, $RuRh_2$ top site, and $RuRh_2$ top site (associated with strain effect).[32] Copyright 2021 Wiley-VCH. (G) Schematic illustration of the synthesis of the RuNi/CQDs-600 electrocatalyst. (H) HAADF-STEM image of RuNi/CQDs-600. (I) The calculated adsorption free-energy diagrams for the Volmer step on the RuNi, Pt, and Ru over various exposed surfaces (001), (101), (100), and (111) with H coverage of 1 ML (ML = monolayer).[33] Copyright 2020 Wiley-VCH. (J) Schematic illustration for preparation of RuBi SAA/Bi@OG. (K) Aberration-corrected HAADF STEM image of RuBi SAA/Bi@OG. (L) The relationship between local charge redistribution of Ru nanoparticle and its ΔG_{H^*}.[34] Copyright 2023 Wiley-VCH. HAADF-STEM, high-angle annular dark field-scanning transmission electron microscopy; PLAL, laser ablation in liquid; SAA, single-atom alloy.

Metal element engineering coupled with morphology engineering may further improve the catalytic activity of Ru-related materials toward the alkaline HER. For instance, Cai et al. synthesized nanosheet-structured RuCo alloy (RuCo ANSs) via co-precipitation coupled with an electrochemical reduction strategy.[35] Structural characterizations displayed that the Ru atoms were individually implanted into the co-host with plane-symmetric structures in the *X* and *Y* directions, while asymmetric structures in the *Z* direction, resulting in optimized electronic properties (Figure 4A,B). Moreover, the binding energy of Ru-H in RuCo ANSs was remarkably increased

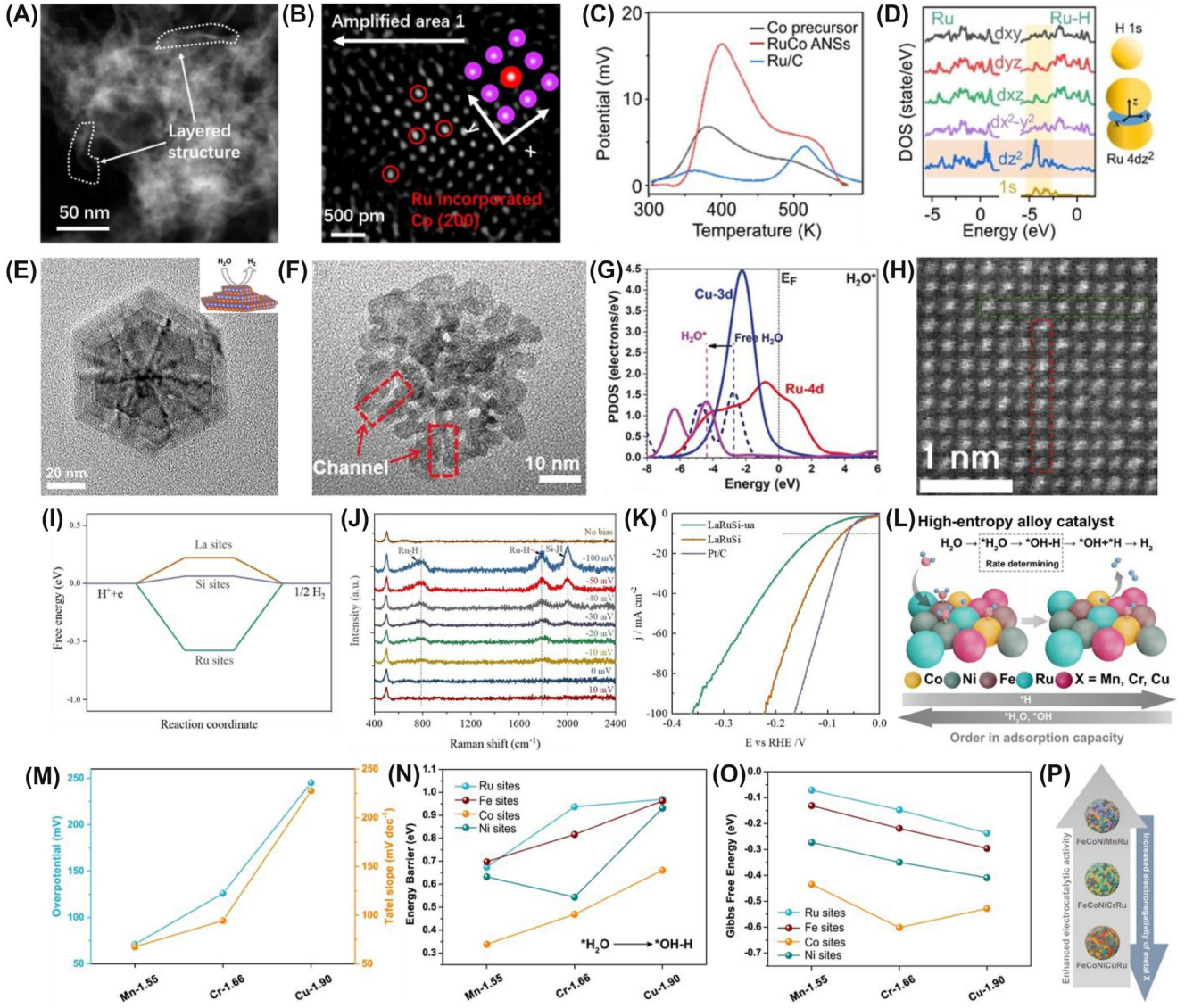

FIGURE 4 (A) STEM image and (B) atomic structure of Ru-substituted Co (200) of RuCo ANSs. (C) TPD tests of Co precursor, RuCo ANSs, and Ru/C. (D) The PDOS of Ru 4d orbitals before and after H* adsorption.[35] Copyright 2022 Wiley-VCH. (E) High-magnification TEM image of an individual RuNi NS.[36] Copyright 2019 Elsevier. (F) High-magnification TEM image of RuCu NSs. (G) The PDOS of H_2O adsorption on RuCu NSs.[37] Copyright 2019 Wiley-VCH. (H) HR-STEM image of LaRuSi. (I) H adsorption-free energy at different sites of LaRuSi. (J) In situ Raman spectra of the LaRuSi catalyst at various potentials (vs. RHE) under HER conditions in 1 M KOH. (K) LSV curves of LaRuSi-ua, LaRuSi, and Pt/C in 1 M KOH.[38] Copyright 2022 Wiley-VCH. (L) Schematic illustration of HEA electrocatalysts with identified electronegativity-dependent preferences for active site adsorption of the intermediates OH* and H* during H_2O dissociation and H_2 production steps. (M) Correlation between the HER overpotentials at 100 mA cm^{-2}, Tafel slopes, and the electronegativities of metals X (Cr, Mn, and Cu). (N) Correlation between the energy barrier for H_2O dissociation at different metal sites and the electronegativities of metals (Cr, Mn, and Cu). (O) Correlation between ΔG_{H^*} at different metal sites and the electronegativities of metals X (Cr, Mn, and Cu). (P) Adjustment of the HER activities of HEA electrocatalysts by tailoring the electronegativity of the composition.[39] Copyright 2022 Springer Nature. HEA, high entropy alloys; HER, hydrogen evolution reaction; HR-STEM, high-resolution scanning transmission electron microscopy; LSV, linear sweep voltammetry; PDOS, projected density of states; RHE, reversible hydrogen electrode; TEM, transmission electron microscopy; TPD, temperature program desorption.

in comparison with Ru nanoparticles (Figure 4C). Consequently, the RuCo ANSs showed an overpotential as low as 10 mV at 10 mA cm^{-2} in the alkaline electrolyte, superior to Pt/C. Density functional theory (DFT) demonstrated that the binding energy of Ru-H was essentially induced by the robust interaction between the Ru $4dz^2$ and the H 1s (Figure 4D). Furthermore, the electron redispersion between Ru sites and Co properly lowered the d-band center of Ru, thus optimizing the adsorption/desorption behavior of H intermediate in the RuCo ANSs. Liu et al. designed a RuNi alloy with unique multilayered nanosheet nanostructures (RuNi NSs) via a one-pot solvothermal method (Figure 4E).[36] They found that the RuNi NSs delivered lower overpotential of 15 mV compared to the commercial Ru/C (70 mV) and Pt/C (54 mV) at 10 mA cm^{-2} for the alkaline HER, which was due to its high active surface area; moreover, the incorporation of Ni atoms induced the optimization of water cleaving and hydrogen adsorption/desorption behavior on the RuNi NSs surface. Yao et al. constructed channel-rich RuCu nanosheets (RuCu NSs) by a wet chemical strategy, which was made up of crystallized Ru, amorphous Cu, and abundant approachable channels (Figure 4F).[37] It is worth noting that, such rich channels contributed to providing enough effective surface area and accelerating the transportation of mass for improving the electrocatalytic activity. Hence, the RuCu NSs displayed a low overpotential of 20 mV for the alkaline HER relative to Pt/C (60 mV) at 10 mA cm^{-2}. Theoretical calculations exhibited that the wide range of electron-rich Ru 4d bands and electron-rich Cu 3d bands were beneficial to the stabilization of charge redistribution between Ru and reaction intermediates. Moreover, the lowered H 1s and H_2O 2p bands confirmed the strong adsorption to promote the alkaline HER process (Figure 4G).

Many previous studies have indicated that the reaction sites of Ru-related catalysts are mainly Ru sites, but unusual active sites may also appear. For example, Shen et al. prepared LaRuSi catalyst by arc melting combined with rapid annealing treatment (Figure 4H).[38] Experimental measurements combined with theoretical calculations confirmed that the actual active sites toward the alkaline HER in LaRuSi system were Si sites, rather than the commonly hypothetical Ru sites. However, the hydrogen adsorption energy on Si sites approached zero (Figure 4I). Moreover, the proper hydrogen adsorption on Si sites during the alkaline process was also confirmed by in situ Raman characterization (Figure 4J). As a result, the LaRuSi showed good activity with a low overpotential of 72 mV at a current density of 10 mA cm^{-2}, approaching Pt/C (Figure 4K).

Comparing alloys with few elements, high entropy alloys (HEA) can easily achieve multiple active sites to acquire highly active, durable, and economical electrocatalysts through ingenious element regulation. Hao et al. designed a FeCoNiXRu (X: Cu, Cr, and Mn) HEA catalyst by using a polymer nanofiber reactor strategy, which possessed two categories of active sites with different adsorption energy for different reaction intermediates (Figure 4L).[39] Operando electrochemical Raman spectra combined with theoretical calculations confirmed that the Co sites were the water dissociation sites, while the Ru sites were the hydrogen adsorption/desorption sites in the FeCoNiMnRu HEA (Figure 4M–O). More importantly, the catalytic activities of HEA catalysts could be accurately regulated by altering the electronegativities of the elements (Figure 4P). Overall, metal element engineering was demonstrated to be a promising approach to constructing highly active Ru-related catalysts for the alkaline HER.

2.1.2 | Nonmetal element engineering

Owing to the high electronegativity of nonmetal elements, nonmetal element engineering can greatly alter the local coordination environment of Ru sites through the formation of Ru-nonmetal element bonds.[40,41] For example, Zhao et al. properly altered the electronic properties of the Ru surface by deliberately introducing P into the lattice to greatly improve electrocatalytic activity for the alkaline HER (Figure 5A).[40] The optimal P-Ru/C showed an overpotential of 31 mV at 10 mA cm^{-2}, smaller than that of Ru/C (103 mV) and Pt/C (39 mV). Experimental and DFT results presented that the increased activity was due to the electronic regulation of the P dopant (Figure 5B,C). Except for the single element doping, the dual atom doping can further increase the catalytic activity of Ru-related catalysts toward the HER in an alkaline medium. Our group incorporated both P and Mo atoms into Ru nanoparticles supported on P-doped carbon substrate (named as P,Mo-Ru@PC) by the confinement effect of metal–organic frameworks (Figure 5D).[27] The P,Mo-Ru@PC displayed a lower overpotential of 21 to reach 10 mA cm^{-2} relative to Pt/C (33 mV) toward the alkaline HER. Profiting from the low Ru content of 1.8 wt%, its mass activity was 22-fold higher than that of Pt/C. Theoretical calculations indicated that doping engineering effectively promoted electron redispersion on the Ru sites, thus, lowering the reaction energy barrier toward the alkaline HER (Figure 5E–G). Liu et al. prepared S-doped RuP nanoparticles uniformly anchored on tri-elements-doped carbon nanosheet (S-RuP@NPSC) with ultralow Ru loading of 0.8 wt%, which delivered a 22.88 times higher mass catalytic activity than that of Pt/C (Figure 5H).[41] Interestingly, both

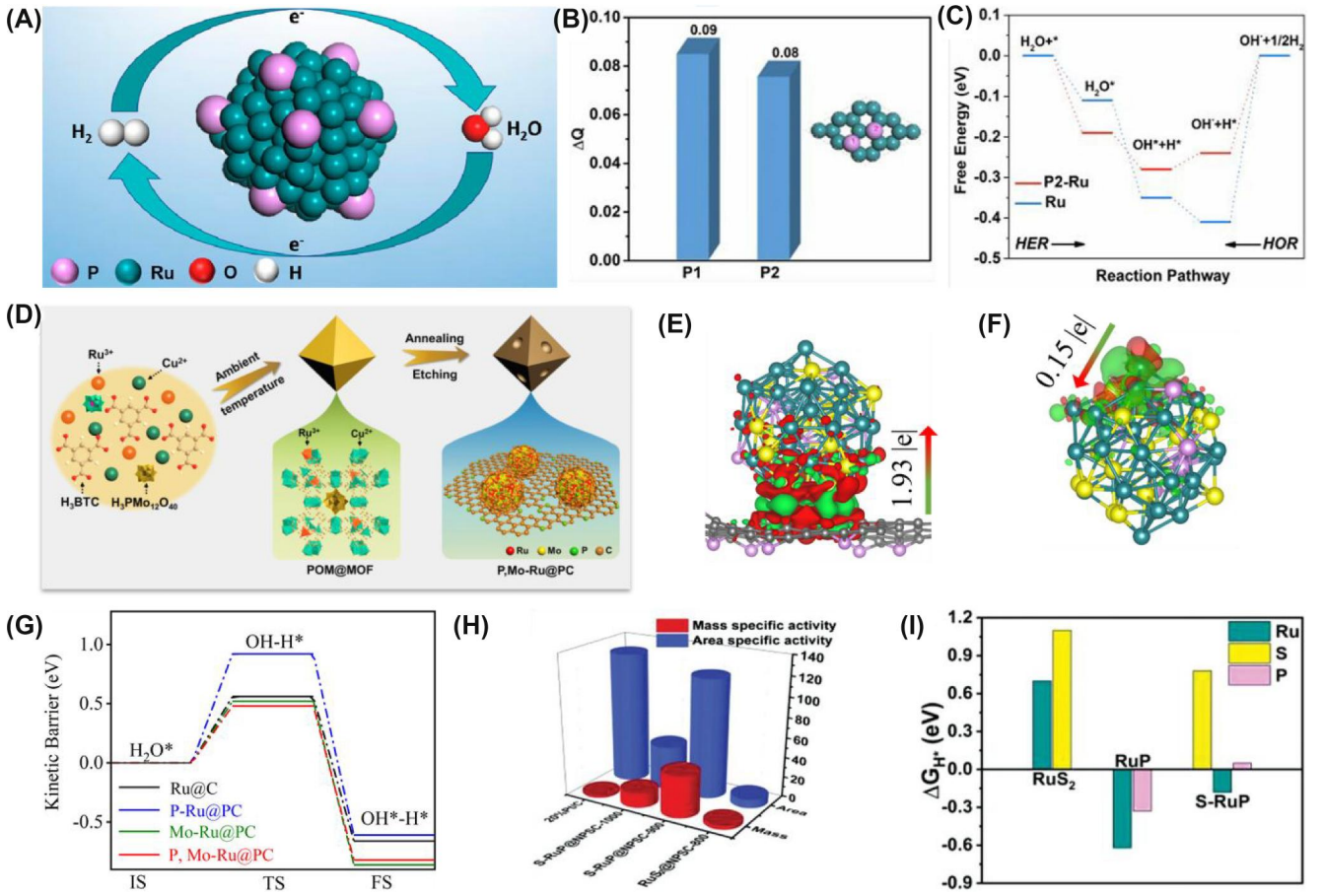

FIGURE 5 (A) Schematic illustration of P-Ru/C. (B) The Bader charge analysis. (C) Reaction paths of P2-Ru and Ru toward the alkaline HER.[40] Copyright 2020 American Chemical Society. (D) Schematic illustration of the synthetic strategy of P,Mo-Ru@PC. (E) The differential charge density distributions between P,Mo-Ru clusters and PC with the isovalue of 0.002 e Å^{-3}. Red represents positive charges and green represents negative charges. (F) Differential charge density distributions for selected single Ru atom in P,Mo-Ru cluster with the isovalue of 0.002 e Å^{-3}. (G) The kinetic barrier of water dissociation on the active sites of different catalysts.[27] Copyright 2022 Wiley-VCH. (H) The mass-specific activity of S-RuP@NPSC. (I) The Gibbs free energy of H* adsorption (ΔG_{H^*}) on various sites.[41] Copyright 2020 Wiley-VCH. HER, hydrogen evolution reaction.

the surface Ru and P sites were demonstrated to act as active sites toward the alkaline HER by the theoretical calculations (Figure 5I). Moreover, the S and P remarkably adjusted the electronic performance of Ru, thus, increasing the reaction activity of Ru-related materials for HER in the alkaline electrolyte. Similar to P and S elements, boron (B) is also an effective nonmetal element to alter the electronic and structural performance of Ru-related electrocatalysts. Qiao et al. found that the introduction of electron-deficient B element could greatly alter the local electronic structure around Ru-B bonds, thus, enhancing the adsorption capacity of H intermediates on Ru atoms in Ru_2B_3 and endowing an ultralow overpotential of 7 mV at 10 mA cm^{-2} in 1 M KOH for Ru_2B_3.[74] Thus, nonmetal element engineering can greatly increase the activity of Ru-related catalysts by optimizing the local coordination environment through unique Ru-nonmetal element bonds.

2.1.3 | Heterostructure engineering

Combining the Ru component with foreign metals, metal oxides, metal carbide, and so on, to construct heterostructures can effectively promote the electronic redistribution at the heterointerface, which will significantly optimize the adsorption energy of reaction intermediates to enhance the reaction kinetics for the alkaline HER.[42–44] For instance, Tu et al. prepared a heterostructure composed of RuMo nanoalloys and N-doped carbon substrates through a hard-templating synthesis combined with an anion-exchange strategy (Figure 6A,B).[42] When acted as a catalyst for the alkaline HER, such heterostructure exhibited an overpotential of 18 mV to reach 10 mA cm^{-2} and a superior turnover frequency of 3.57 H_2 s^{-1}, which is much superior to Pt/C (32 mV, 0.02 H_2 s^{-1}). DFT calculations presented that the N dopant in the carbon matrix and the Mo dopant in Ru

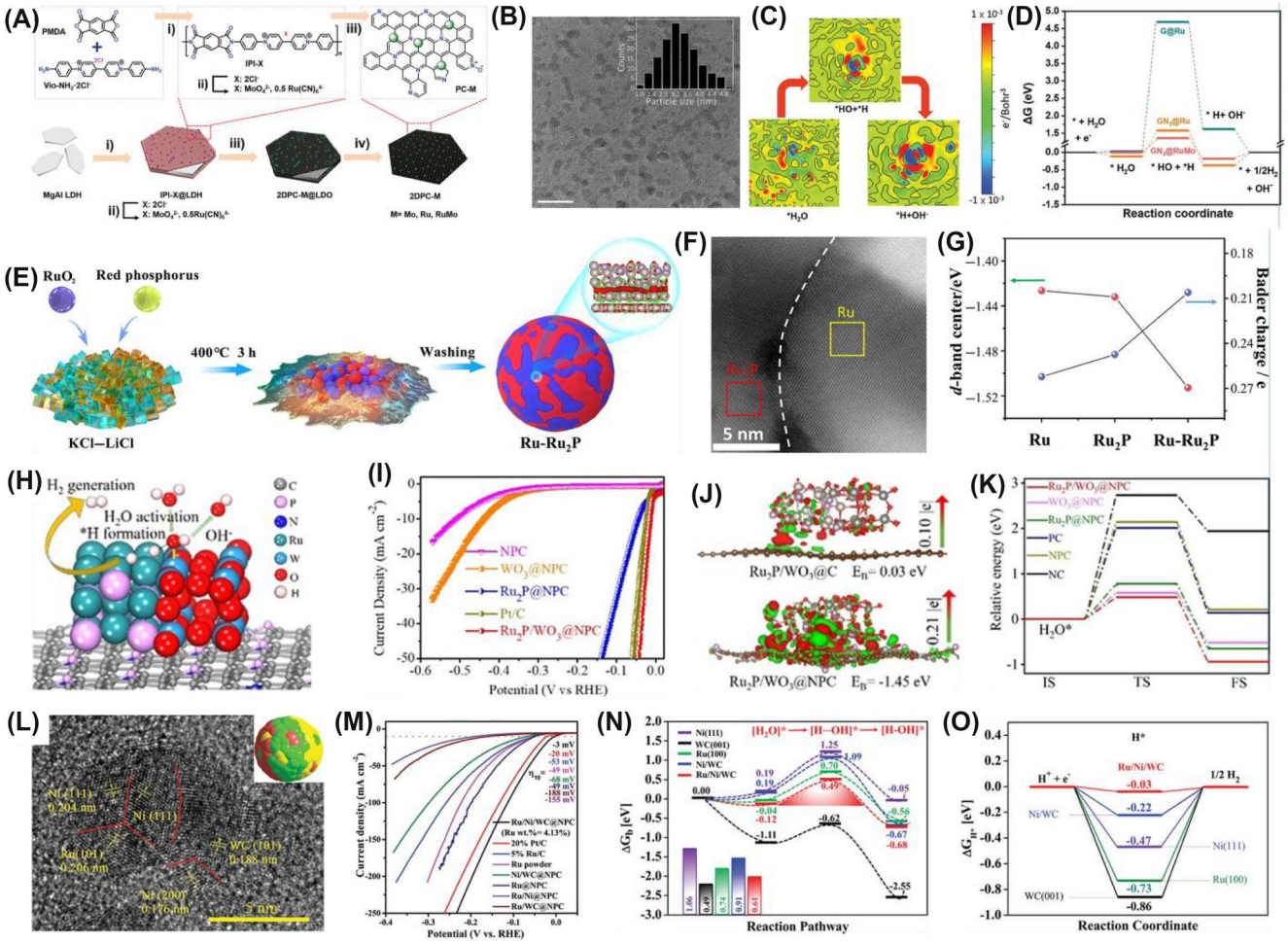

FIGURE 6 (A) A schematic fabrication procedure of metal-composite-embedded hexagonal porous carbon nanosheets. (B) High-resolution TEM image of the 2DPC-RuMo nanosheets. Scale bar: 10 nm. (C) 2D charge difference isosurfaces for the HER path on GN_4@RuMo. (D) Free energy profile for GN_3@RuMo, GN_3@Ru, and G@Ru along the reaction pathway.[42] Copyright 2020 Wiley-VCH. (E) Schematic illustration of the fabrication of Ru-Ru_2P. (F) AC-STEM image of Ru-Ru_2P-4. (G) Relationship between the d-band center of electrocatalysts and the Bader charge of adsorbed H.[43] Copyright 2022 Wiley-VCH. (H) Proposed HER mechanism in alkaline media for the Ru_2P/WO_3@NPC nanocomposite. (I) LSV curves of Ru_2P/WO_3@NPC, Ru_2P@NPC, WO_3@NPC, NPC, and commercial Pt/C (20 wt%). (J) Charge density distributions between Ru_2P/WO_3 and different substrates (C, NPC) with a value of 0.002 e $Å^{-3}$. (K) Kinetic barriers of water dissociation on the active sites of Ru_2P/WO_3@NPC, Ru_2P@NPC, WO_3@NPC, NPC, PC, and NC.[44] Copyright 2021 Wiley-VCH. (L) HRTEM images of Ru/Ni/WC@NPC (Ru wt% = 4.13%). Inset of the model of Ru/Ni/WC nanoparticle. (M) Electrocatalytic properties evaluation of HER in 1 M KOH at ambient conditions. (N) Gibbs free energy profile for water dissociation on those designed models. (O) Computed free energy diagram for H adsorbed on different surfaces.[45] Copyright 2022 Wiley-VCH. AC-STEM, spherical aberration-corrected scanning transmission electron microscopy; HRTEM, high-resolution transmission electron microscopy; LSV, linear sweep voltammetry; TEM, transmission electron microscopy.

lattices highly motivate the electronic aggregation/loss at the heterointerface, thus, decreasing the reaction energy barrier and accelerating the reaction rate toward the HER process in an alkaline condition (Figure 6C,D). Chen et al. produced a homologous metallic Ru-Ru_2P heterostructure catalyst by using a salt-assisted catalytic synthesis method (Figure 6E,F).[43] The as-prepared Ru-Ru_2P possessed abundant heterojunction interfaces, delivering a lower overpotential of 18 mV for the alkaline HER at 10 mA cm^{-2}, outperforming the activity of Pt/C (37 mV). DFT results exhibited that there was an effective charge repartition at the rich heterointerface of Ru-Ru_2P, which lowered the d-band orbit and increased the adsorption strength of the reaction intermediates for the alkaline HER (Figure 6G).

Furthermore, the multi-interfacial feature of multi-component heterostructures can further optimize the binding energy of the reaction intermediate species toward the alkaline HER. Our group designed a Ru_2P/WO_3@NPC heterostructure through a hydrothermal reaction coupled with the pyrolysis strategy (Figure 6H).[44] The Ru_2P/WO_3@NPC as HER catalyst in an alkaline

medium exhibited a lower overpotential of 15 mV to reach 10 mA cm^{-2} relative to benchmark 20 wt% Pt/C (23 mV, Figure 6I). DFT calculations coupled with experimental measurements demonstrated that there was the transportation of electrons not only from NPC to Ru_2P/WO_3 but also from Ru_2P to WO_3, greatly promoting the charge redistribution at the multi-interface of Ru_2P/WO_3@NPC (Figure 6J). Therefore, such electron density redistribution induced the enhancement of water dissociation capacity on W sites and hydrogen desorption capacity on Ru sites (Figure 6K). In addition, Salah et al. prepared a multi-heterostructure catalyst (Ru/Ni/WC@NPC) toward the alkaline HER through a hydrothermal combined with the pyrolysis method (Figure 6L).[45] With an ultralow Ru content of 4.13 wt%, such catalyst displayed a state-of-the-art activity with an ultralow overpotential of 3 mV at 10 mV cm^{-2} in comparison with Pt/C (20 mV, Figure 6M). Theoretical calculations indicated the Ru/Ni/WC catalyst with multi-interface possessed superior adsorption/dissociation capacity for water and near-zero adsorption energy for hydrogen, owing to its weak exothermic effect (Figure 6N,O). Overall, the formation of heterostructures could induce charge redistribution at interfaces to elevate the activity of Ru-related catalysts.

2.1.4 | Electronic metal–support interaction

The EMSI between metal nanoparticles/single atoms and supports not only can effectively anchor and disperse metal particles but also has a significant effect on the chemical and catalytic performances of metal-based catalysts.[75–77] Among various support materials, carbon materials are extensively applied due to their superior conductivity and low cost. Li et al. prepared Ru nanoparticles evenly anchored on graphene nanoplatelets (Ru@GnP) via a mechanochemically assisted strategy (Figure 7A).[46] Satisfactorily, Ru@GnP displayed a lower overpotential of 22 mV at 10 mA cm^{-2} compared to commercial Pt/C (33 mV). In addition, after the structural and composition modification of carbon supports, the catalytic performance of the supported catalyst can be further increased. Ye et al. constructed Ru nanoclusters well distributed on B- and N-codoped graphene (Ru NCs/BNG) by a simple pyrolyzation strategy (Figure 7B).[47] It is worth noting that, the B element played a decisive role in the generation of ultrafine Ru nanoparticles (0.5–1 nm) on the carbon matrix. As a result, the B doping remarkably enhanced the catalytic activity of Ru NCs/BNG in comparison with Ru NCs/NG for the alkaline HER. Moreover, the Ru NCs/BNG exhibited an overpotential of 14 to reach 10 mA cm^{-2}, superior to Pt/C (26 mV, Figure 7C). More importantly, the stability of Ru NCs/BNG was much superior to Pt/C (Figure 7D). They thought that the electronic mutual effect between Ru nanoclusters and boron atoms greatly promoted the dissociation of water, thus, regulating the reaction mechanism and reducing the formation energy barrier of hydrogen (Figure 7E).

In addition to introducing nonmetal elements, the incorporation of single atoms into the carbon framework would alter the π-conjugated properties of carbon supports to improve the EMSI between carbon carriers and Ru nanoparticles. Su et al. found that the individually single atom embedded in the carbon matrix induced a synergistic electron effect around metal nanoparticles, enhancing the interaction between the metal nanoparticles to accelerate reaction kinetics for the alkaline HER (Figure 7F).[48] Firstly, theoretical calculations indicated that the introduction of atomically dispersed metal species into O-doped graphene substrate not only greatly increased the EMSI between Ru nanoparticles and carrier but also promoted the charge redistribution of Ru species, thus, resulting in the optimization of hydrogen adsorption energy on Ru active sites to improve the HER activity (Figure 7G). Directed by DFT results, they designed a supported catalyst with Ru nanoparticles anchored on Co and oxygen-codoped graphene (Ru/Co@OG) by using a salt-template strategy (Figure 7H). When tested as the alkaline HER catalysts, the Ru/Co@OG delivered a lower overpotential of 13 mV to reach 10 mA cm^{-2} relative to Ru/OG (48 mV) and commercial Pt/C (31 mV) as shown in Figure 7I. In a word, the coupling of single metal atoms in carbon substrate was demonstrated to be an effective means to optimize the electronic properties of Ru nanoparticles by increasing the EMSI between the supported Ru nanoparticles and the support.

In comparison with the carbon substrates, the metal oxide carriers are inclined to generate more robust interaction with the Ru nanoparticles at the contact interface, thus, significantly enhancing the catalytic performance. Moreover, metal oxides possess various advantages, including varying nanostructures, diverse constituents, easy preparation, etc.[78–80] Lately, the supported Ru catalysts on various metal oxide support (Fe_3O_4, TiO_2, SnO_2, HfO_2, MoO_2, CuO, etc.)[49–52,81–83] have been widely explored and exhibited high catalytic performance toward the alkaline HER, owing to the robust EMSI between Ru metal nanoparticles and metal oxide supports. For example, Li et al. prepared Ru nanoparticles dispersed on Fe_3O_4 anchored on carbon matrix (Ru-Fe_3O_4/C) through a hydrothermal coupled with heat treatment method (Figure 8A).[49] They thought that the self-accommodation of Ru nanoparticles on the Fe_3O_4 surface, not the carbon matrix surface, was due to

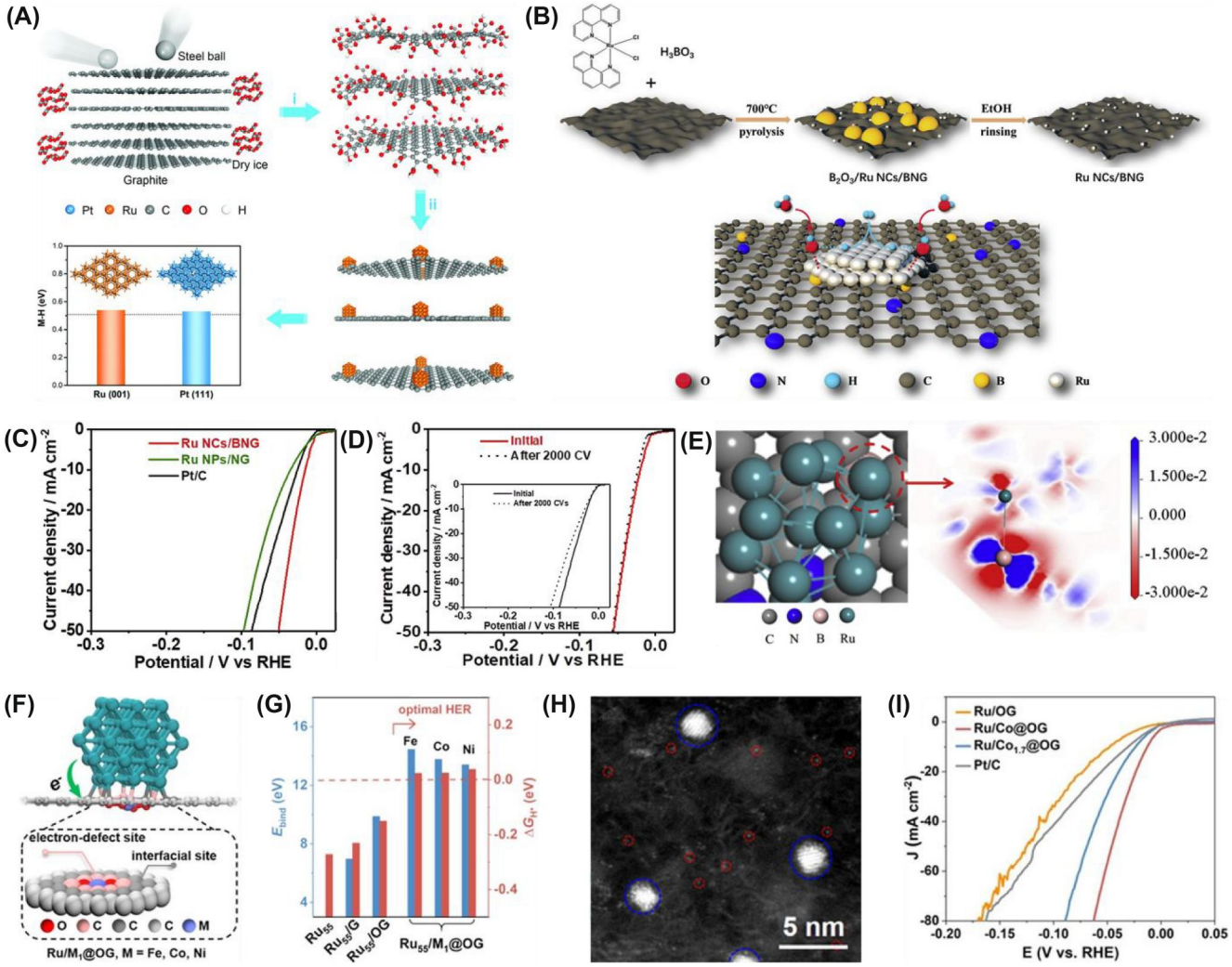

FIGURE 7 (A) Schematic illustration of the synthesis and theoretical calculation of Ru@GnP.[46] Copyright 2018 Wiley-VCH. (B) Synthesis and structure of Ru NCs/BNG. (C) LSV curves of Ru NCs/BNG, Ru NPs/NG, and Pt/C with current density normalized to the geometry of the electrode in 1 M KOH at 2 mV s^{-1} with iR correction. (D) LSV curves of Ru NCs/BNG before and after 2000 cycles in 1 M KOH at 2 mV s^{-1}. Inset of the LSV curves of Pt/C before and after 2000 cycles in 1 M KOH at 2 mV s^{-1}. (E) The calculation model (top view) and corresponding electronic density difference at the interface were highlighted by the red circle.[47] Copyright 2020 Elsevier. (F) Atomic structures of Ru_{55} supported on O-doped graphene with dispersed metal atoms obtained by DFT calculations. (G) Binding energies (E_{bind}, left axis) of Ru_{55}/M_1@OG and freestanding Ru_{55}, and its corresponding adsorption free energy of H* species (ΔG_{H^*}, right axis). (H) HAADF-STEM image for Ru/Co@OG electrocatalysts. (I) LSV curves of Ru-based catalysts and commercial Pt/C.[48] Copyright 2021 Wiley-VCH. DFT, density functional theory; HAADF-STEM, high-angle annular dark field-scanning transmission electron microscopy; LSV, linear sweep voltammetry.

the strong EMSI. Experimental evidence and DFT results confirmed that there was electronic perturbation in the system of Ru-Fe_3O_4/C and the emergence of electron redistribution greatly optimized the adsorption energy of reaction intermediates for the HER in an alkaline condition (Figure 8B). The formation of Ru-O bands induced by the orbital overlap greatly altered the electron density around Ru sites to transfer more electrons to hydrogen intermediates, which was beneficial for the adsorption behavior during the HER process. Moreover, the antibonding property of hydrogen intermediates was strengthened due to the weak binding strength of the Ru-O bonds, enabling the easy formation behavior of H_2 molecules (Figure 8C). Consequently, the Ru-Fe_3O_4/C delivered a superior catalytic activity with an overpotential of 11 mV to arrive at a current density of 10 mA cm^{-2}, better than that of Pt/C benchmark (17 mV) in the alkaline electrolyte. Chen et al. synthesized Ru nanoparticles on reduced TiO_2 with rich oxygen vacancies (Ru/r-TiO_2) by the robust reductive effect of newly produced Ti(III) oxide (Figure 8D).[50] The Ru/r-TiO_2 showcased a smaller overpotential of 15 mV to arrive at a current density of 10 mA cm^{-2} relative to Ru/TiO_2 without oxygen vacancies (32 mV) and

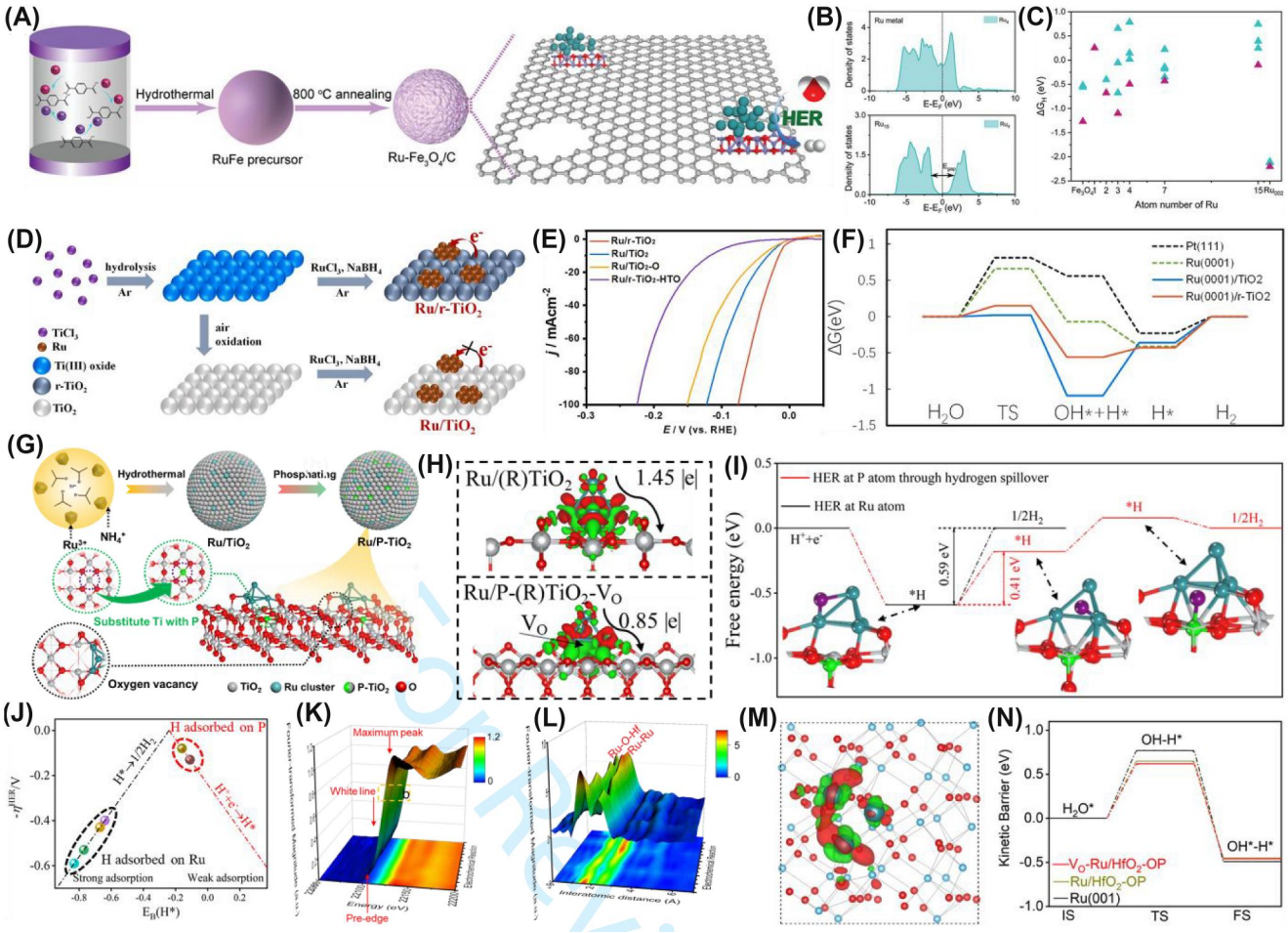

FIGURE 8 (A) Synthesis scheme of Ru-Fe_3O_4/C and its corresponding application toward the HER. (B) Partial density of states of the Ru d-orbital of Ru metal and Ru nanoparticle (15 elements) on Fe_3O_4. EF indicates the Fermi level. (C) Calculated $\Delta G_{H's}$ from Fe_3O_4, Ru nanoparticle on Fe_3O_4, and pure Ru metal.[49] Copyright 2023 Wiley-VCH. (D) Schematic illustration of the synthesis of Ru/r-TiO_2 and Ru/TiO_2 catalysts. (E) HER polarization curves of Ru/r-TiO_2, Ru/TiO_2, Ru/TiO_2-O, and Ru/r-TiO_2-HTO electrocatalysts in H_2-saturated 1.0 M KOH solution. (F) Free energy profiles for HER from aqueous water to H_2 on different surfaces.[50] Copyright 2021 Elsevier. (G) Schematic representation of the preparation of Ru/P-TiO_2 catalyst. (H) The differential charge density distributions between adsorbed Ru and R-TiO_2, Ru and P-(R)TiO_2-VO (down) with the isovalue of 0.008 e $Å^{-3}$. Red represents negative charges and green represents positive charges. (I) The Gibbs free energy diagram for HER at Ru atom (dark line) and P atom through hydrogen spillover pathway (red line) for Ru/P-(R)TiO_2-VO. (J) Volcano plot of theoretical overpotential for the hydrogen evolution reaction (HER) relative to standard hydrogen electrode (η_{HER}) versus the binging energy of H atom (EB) on Ru or P atoms of different catalysts.[51] Copyright 2022 Wiley-VCH. (K) Three-dimensional plot of operando Ru K-edge XANES spectrum recorded at varied potential from OCV to −0.6 V (vs. RHE) during the HER catalysis. (L) Three-dimensional plot of operando Ru K-edge FT-EXAFS spectrum of VO-Ru/HfO_2-OP. (M) The differential charge density distributions between Ru_3 clusters and VO-HfO_2 with the isovalue of 0.001 e $Å^{-3}$. (N) Kinetic barrier of water dissociation on the active sites of VO-Ru/HfO_2-OP, Ru/HfO_2-OP, and Ru(001).[52] Copyright 2022 Springer Nature. RHE, reversible hydrogen electrode.

Pt/C (34 mV) toward the HER in alkaline conditions (Figure 8E). Experimental results combined with DFT calculations revealed that the existence of rich oxygen vacancies led to the generation of more negatively charged Ru sites. They also found that the greatly enhanced catalytic activity for the alkaline HER was attributed to the heightened water dissociation capacity and weakened OH adsorption capacity, which was induced by the existence of reduced TiO_2 (Figure 8F).

I, the introduction of other elements into metal oxides can also optimize the charge redistribution at the interface to alter the coordination environment between Ru nanoparticles and metal oxide supports, which further impresses the catalytic performance of supported Ru catalysts. For example, our group prepared Ru clusters dispersed on defective TiO_2 with trace P dopant (Ru/P-TiO_2) by a hydrothermal reaction with subsequent phosphorization treatment (Figure 8G).[51] When acted as the cathodic catalyst for the alkaline HER, the

as-prepared Ru/P-TiO_2 exhibited Pt-like activity with a lower overpotential of 27 mV to arrive at a current density of 10 mA cm^{-2} compared to Ru/TiO_2 (85 mV). Its mass activity (9984.3 mA mg_{Ru}^{-1}) was also 34.3 times greater than that of Pt/C. Experimental measurements and theoretical calculations showed the TiO_2 support with the rutile phase displayed a higher activity for the alkaline HER than that with the anatase phase. Moreover, the oxygen vacancies could induce the inversion of the electron-transfer direction to produce charge-rich Ru nanoclusters in Ru/P-(R)TiO_2-VO, thus, enhancing the H_2O dissociation capacity (Figure 8H). More importantly, the introduction of P^{5+} at the position of Ti^{4+} would further synergistically improve the catalytic activity for the alkaline HER, which was attributed to the accelerated formation of H_2 molecule induced by the H* spillover from the Ru site to the P site at the system surface (Figure 8I,J).

In addition, distinguishing the contribution of HER activity between Ru nanoparticles and metal oxide substrates for supported catalysts with strong EMSI is significant and desired. Our group prepared Ru nanoparticles anchored on HfO_2 (Ru/HfO_2) by using a hydrothermal reaction combined with a thermal reduction treatment method.[52] Owing to the high band gap over 5 eV of HfO_2, the activity contribution between Ru nanoparticles and HfO_2 carrier was well distinguished. When served as catalysts for the alkaline HER, the pristine HfO_2 was inert even at strong applied voltages, while optimal Ru/HfO_2 delivered a superior catalytic activity with a low overpotential of 39 mV at 10 mA cm^{-2} closed to Pt/C. Moreover, the mass activity of optimal Ru/HfO_2 was 20-fold higher than that of commercial Pt/C. Operando XAS measurements revealed that the structural distortions and reversible valence change of Ru in Ru/HfO_2 were elastic, which contributed to the enhancement of catalytic performance (Figure 8K,L). Charge density difference analysis indicated that there was strong EMSI between Ru nanoclusters with HfO_2 substrate with electron transfer from Ru to HfO_2 (Figure 8M). Experimental and theoretical data expounded that the activity of Ru/HfO_2 was adjusted by the amount of Ru-O-Hf bonds. Moreover, the EMSI induced by Ru-O-Hf bonds coupled with oxygen vacancies greatly increased the water dissociation capacity to accelerate the formation of H_2 (Figure 8N).

Metal–organic frameworks (MOFs) are extremely versatile and ultra-porous nanomaterials that are constituted by varied organic ligands and metal centers, which can be applied to store, separate, and release almost anything.[84–86] Owing to their unique properties, MOFs are deemed to be effective substrates to support metal catalysts. Sun et al. dispersed atomically Ru on Ni-BDC MOF ($NiRu_{0.13}$-BDC) by using a hydrothermal with subsequent ion-exchange method (Figure 9A).[53] Such constructed $NiRu_{0.13}$-BDC displayed a Pt-like activity (34 mV @10 mA cm^{-2}) in an alkaline electrolyte (Figure 9B). Characterization results coupled with DFT calculations showed that there was a charge interaction between Ru and Ni to regulate the electronic performance of the metal center in the MOF (Figure 9C), resulting in greatly optimizing the absorption energy of H_2O and H*, and accelerating the reaction kinetics for the alkaline HER (Figure 9D,E). Other than atomically dispersed Ru, Ru nanoparticles can also be anchored on MOF via the ESMI. Deng et al. fabricated Ru nanoparticles supported on Ni-MOF nanosheet arrays (Ru@Ni-MOF) through a general spontaneous redox reaction method (Figure 9F).[54] Note that the Ni-MOF was chosen as a sinewy substrate to keep Ru nanoparticles from agglomerating to provide enough effective surface active sites for electrochemical reaction. Moreover, there was the generation of Ni-O-Ru bonds that promoted electron transport at the interface to ensure fast reaction kinetics. DFT studies revealed that the electron relocation at the interface was induced by the Ni-O-Ru bonds to optimize the adsorption capacity for H_2O and hydrogen intermediates to accelerate HER kinetics (Figure 9G,H). Consequently, the optimal Ru@Ni-MOF reached 10 mA cm^{-2} only using 22 mV for the alkaline HER, which was smaller than that of the commercial Pt/C (46 mV, Figure 9I). Therefore, the Ru-based supported catalysts with strong ESMI can not only reduce the use of Ru but also improve their activity and stability for the alkaline HER.

2.2 | Geometric modulation

The geometric modulation, including size engineering and phase engineering strategies can determine the properties and functionalities of nanomaterials.[87–89]

2.2.1 | Size engineering

With the booming development of surface science, extensive efforts indicate that the unsaturated coordination environment of Ru species will increase with the decrease in metal size. Therefore, size engineering can effectively alter the catalytic performance of Ru-related nanomaterials toward the alkaline HER.[89] To analyze the role of single Ru atoms and Ru nanoparticles as catalytic active sites toward HER, our group constructed both Ru single atoms and nanoparticles dispersed on defect-rich carbon substrate (Ru_{SA+NP}/DC) by using a

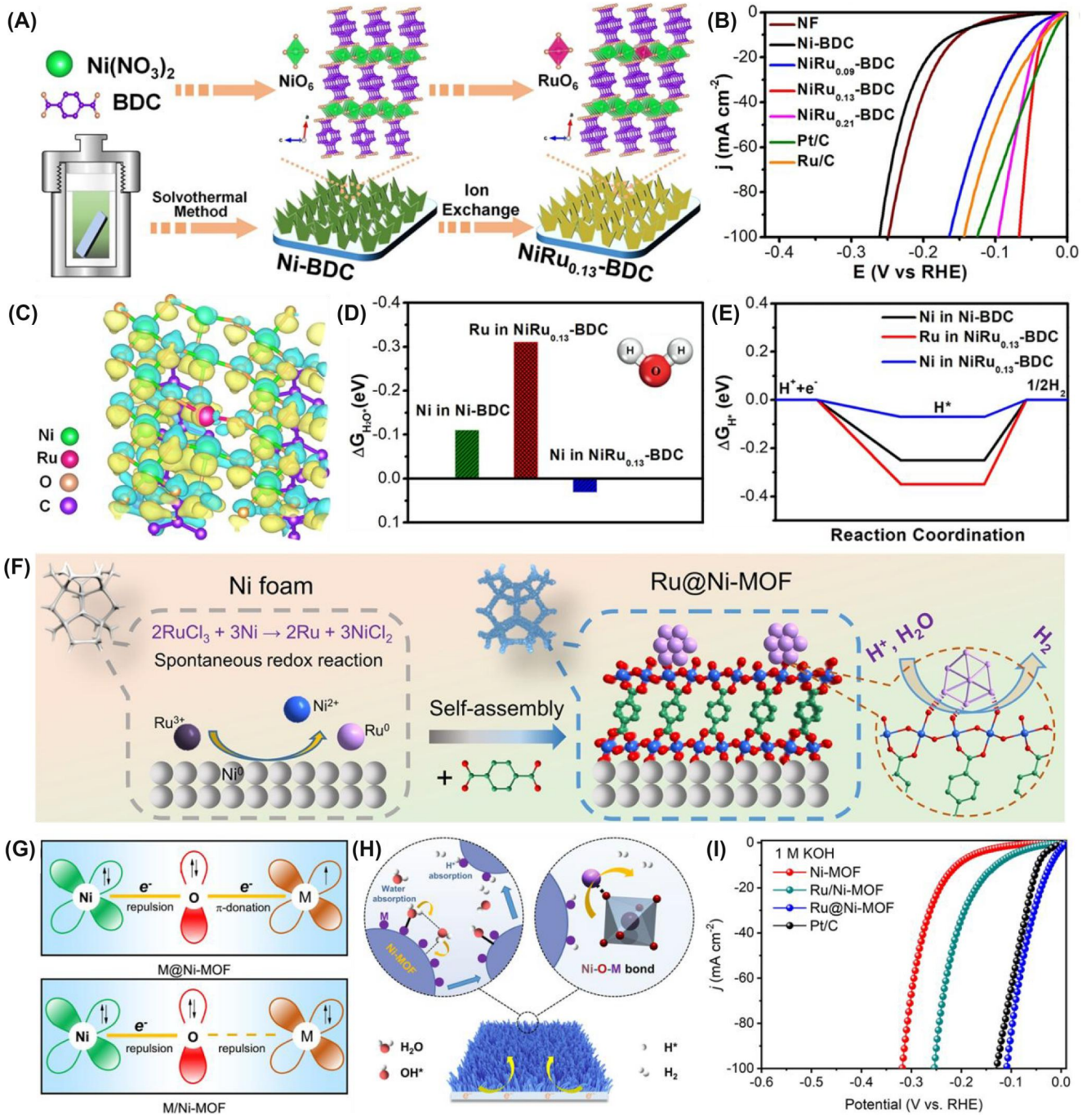

FIGURE 9 (A) Schematic illustration for the preparation of $NiRu_{0.13}$-BDC catalyst. (B) LSV curves toward HER of Ni-BDC, $NiRu_{0.09}$-BDC, $NiRu_{0.13}$-BDC, and $NiRu_{0.21}$-BDC in 1 M KOH. (C) The charge density difference between Ni-BDC and $NiRu_{0.13}$-BDC. (D) The calculated adsorption free energy of water on Ni-BDC and $NiRu_{0.13}$-BDC. (E) Calculated free energy diagram of the HER.[53] Copyright 2021 Springer Nature. (F) Schematic illustration of the formation of Ru@Ni-MOF nanosheets supported on Ni foam for HER. (G) Schematic diagram of electron transfer of M@Ni-MOF and M/Ni-MOF (M = Ru, Ir, Pd). (H) Schematic illustration of the mechanism of enhanced HER activity on M@Ni-MOF nanosheet arrays. (I) LSV polarization curves in 1.0 M KOH electrolyte for Ru@Ni-MOF, Ru/Ni-MOF, Ni-MOF, and commercial Pt/C (20% Pt).[54] Copyright 2021 Wiley-VCH. LSV, linear sweep voltammetry.

metal-organic supramolecules transformation strategy (Figure 10A).[55] Accordingly, the as-obtained Ru_{SA+NP}/DC displayed superior catalytic activity in alkaline and acidic conditions for HER, which had low overpotentials of 18.8 and 16.6 mV to reach 10 mA cm^{-2}, respectively. Experimental data revealed that the amount of single Ru atoms increased after the HER process in acidic electrolyte while the amount of Ru nanoparticles elevated after

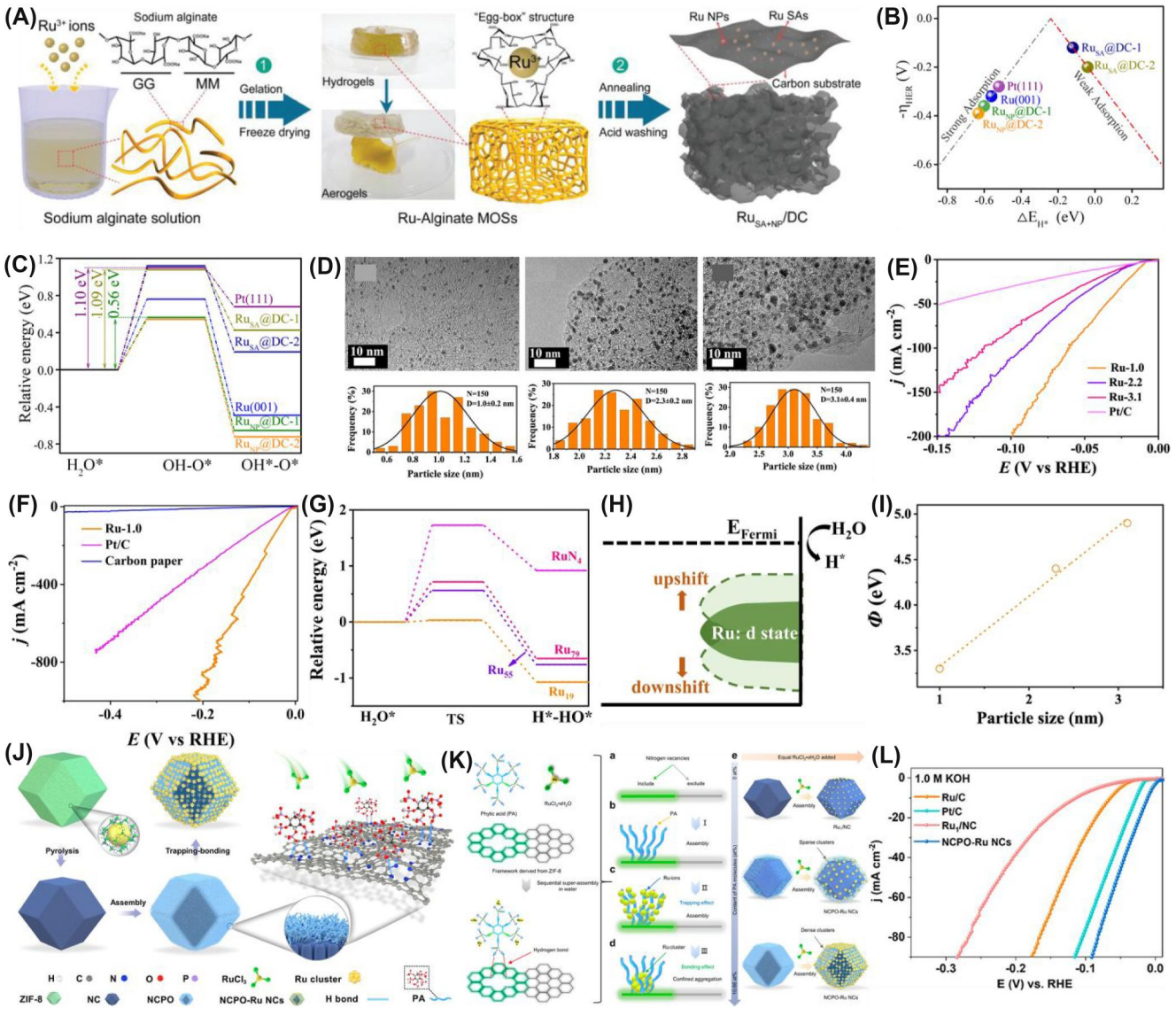

FIGURE 10 (A) Schematic diagram of the synthetic route for Ru_{SA+NP}/DC electrocatalyst. (B) Volcano plot of theoretical η_{HER} versus ΔE_{H^*}. (C) The kinetic barrier of H_2O dissociation for different models.[55] Copyright 2021 Wiley-VCH. (D) TEM images of Ru crystals in different sizes. (E) LSV curves of Ru-1.0, Ru-2.3, Ru-3.1, and commercial Pt/C for HER in 1 M KOH. (F) LSV curves of Ru-1.0, commercial Pt/C, and carbon paper for HER in 1 M KOH. The Ru-1.0 and commercial Pt/C are supported on a carbon paper with a high mass loading of 1 mg cm^{-2}. (G) Kinetic barriers of water dissociation for different Ru cluster models. (H) Schematic illustration of the d band center shift of clusters induced by the particle size that tunes the water dissociation ability. (I) Correlation between particle size and Φ values.[56] Copyright 2022 Springer Nature. (J) Schematics of trapping–bonding strategy for the superassembly of surface-enriched Ru nanoclusters in water. (K) Schematic illustration of the formation mechanism for the NCPO-Ru NCs. (L) HER polarization curves for Ru/C, Pt/C, Ru_1/NC, and NCPO-Ru NCs in 1.0 M KOH.[57] Copyright 2022 American Chemical Society. LSV, linear sweep voltammetry; TEM, transmission electron microscopy.

the HER process in alkaline media. Moreover, DFT results indicated that single Ru atoms mainly contributed to the hydrogen adsorption capacity, while the Ru nanoparticles were dominant to the water dissociation capacity (Figure 10B,C). It is worth noting that, the water-cleaving behavior is the rate-determining reaction toward the alkaline HER. Therefore, the Ru nanoparticles played a dominant role in the formation of H_2 molecules toward the alkaline HER compared to single Ru atoms.

Furthermore, Hu et al. investigated the effect of the physicochemical structure of Ru nanoclusters and Ru nanoparticles on their catalytic performance toward HER in alkaline conditions.[56] They synthesized a series of supported Ru catalysts with different sizes (1, 2.3, and 3.1 nm) on carbon support with the same content of Ru as shown in Figure 10D. When acted as HER catalysts in the alkaline electrolyte, the subnanometric metal clusters Ru-1.0 showed a superior activity with the smallest

overpotential of 13 mV at 10 mA cm^{-2} (Figure 10E). Notably, the prepared electrode on carbon paper also delivered a remarkable activity at 1000 mA cm^{-2} with 196 mV (Figure 10F). Experimental and theoretical results indicated that the energy level of the d-band orbit was closely decided by the size of Ru. The upshifted d-band orbit of the Ru cluster showed its robust H_2O dissociation capacity compared to Ru single atoms and nanoparticles, ensuring the superior HER activity for the Ru cluster (Figure 10G,H). Moreover, the particle size had an efficient effect on the work function values (Φ), also confirming the downtrend of the d band orbit of Ru relative to the uptrend of granular size (Figure 10I). Furthermore, the Ru nanoclusters are demonstrated to be more active for the alkaline HER in comparison with Ru single atoms and nanoparticles.

To make the best of the advantages of Ru nanoclusters, Liang et al. reported surface-enriched Ru nanoclusters on N-doped carbon matrix with the decoration of phytic acid (NCPO-Ru NCs) by using a trapping–bonding method (Figure 10J).[57] The superassembly of Ru nanoclusters at the framework surface was mainly due to the combined action of vacancies and phosphate species. Impressively, the distribution and density of Ru nanoclusters anchored on the framework were also accurately controlled by the change in the amount of phytic acid (Figure 10K). Owing to the surface-enriched Ru nanoclusters with enough exposed active sites, the as-prepared NCPO-Ru NCs arrived at 10 mA cm^{-2} at 11 mV, smaller than that of the commercial Pt/C benchmark (27 mV, Figure 10L). Overall, the Ru nanoclusters were confirmed to be more active than Ru single atoms and nanoparticles for the alkaline HER. Thus, it is an effective means to design advanced Ru-based catalysts toward the alkaline HER by dispersing high-density Ru nanoclusters on special substrates.

2.2.2 | Phase engineering

Phase engineering induced by the rearrangement of the surface Ru atoms can effectively regulate electronic structure to affect their catalytic performance for the alkaline HER.[90] In general, there are two categories of phase for Ru nanomaterials, including face-centered cubic (fcc) and hexagonal close-packed (hcp).[91] Thermodynamically, Ru tends to form the hcp phase, due to the metastable property of the fcc phase. Nevertheless, the fcc phase possesses stronger Ru–Ru bond strength compared to the hcp phase.[92] Thus, the Ru nanomaterials with different phases display different catalytic performances, owing to the diverse atomic arrangements of the fcc and hcp phases. For example, Zheng et al. synthesized two kinds of Ru nanomaterials with an fcc phase and an hcp phase. Impressively, the fcc phase Ru was obtained due to the existence of g-C_3N_4 (Figure 11A).[93] Theoretical calculations further confirmed that the generation of Ru crystal with unusual fcc phase was promoted by the assistance of g-C_3N_4, which was quantitatively analyzed by the defined adhesion energies (ΔE_{adh}) between two Ru crystal phase and g-C_3N_4 support (Figure 11B,C). They also found that the Ru fcc(111) planes were more approachable to the multiple reaction intermediates than that of Ru hcp(0001) planes, which was beneficial for enhancing the hydrogen adsorption capacity and H_2O dissociation capacity (Figure 11D). As a result, the as-prepared unusual Ru nanomaterials exhibited a 2.5-fold faster rate of hydrogen production relative to commercial Pt/C in an alkaline electrolyte. Similarly, Li et al. fabricated the fcc phase Ru nanodendrimers with the embellishment of MoO_x (MoO_x-Ru fcc) by using a colloidal strategy, and the hcp phase Ru nanodendrimers with modification of MoO_x (MoO_x-Ru hcp) through the succedent phase evolution (Figure 11E,F).[94] Electrochemical tests indicated that MoO_x-Ru fcc had a superior catalytic performance in comparison with MoO_x-Ru hcp for the alkaline HER. Moreover, DFT results presented that the decoration of MoO_x greatly increased the structural stability of fcc phase Ru (Figure 11G).

Except for the Ru crystal with pure phase, the multiphase heterostructured Ru catalysts are also found to be remarkably active toward the alkaline HER. For example, Gao et al. designed Ru nanodendrites with fcc/hcp mixed phase, exhibiting a Pt-like activity (43.4 mV@10 mA cm^{-2}).[95] Lu et al. elaborately constructed 4H/fcc Ru nanotubes (4H/fcc Ru NTs) through a sacrificial templates method (Figure 11H).[58] Benefiting from abundant atomic steps at the interface induced by two different crystal structures (fcc/hcp-4H), the local electronic properties of Ru atoms were effectively optimized. Coupled with richly exposed active sites attributed to the hierarchical porous nanostructure, the prepared 4H/fcc Ru NTs arrived at 10 mA cm^{-2} only using 23 mV, smaller than that of the Pt/C benchmark (46 mV, Figure 11I). Moreover, the Ru crystals with superlattices can also endow Ru nanosheets with superior catalytic activity for the alkaline HER, owing to their unique lattice mismatch. Zhang et al. reported the superlattice structured Ru multilayer nanosheets (Ru MNSs) via a wet chemical strategy.[59] Comprehensively, the superlattice structure was produced by the stacked layers with screwy angles of 2°–30° in Ru MNSs (Figure 11J–L). Consequently, such Ru MNSs showed a much lower overpotential of 24 mV at 10 mA cm^{-2} compared to Pt/C (70 mV, Figure 11M). DFT calculations manifested that the superlattice structure resulted in compressed lattice

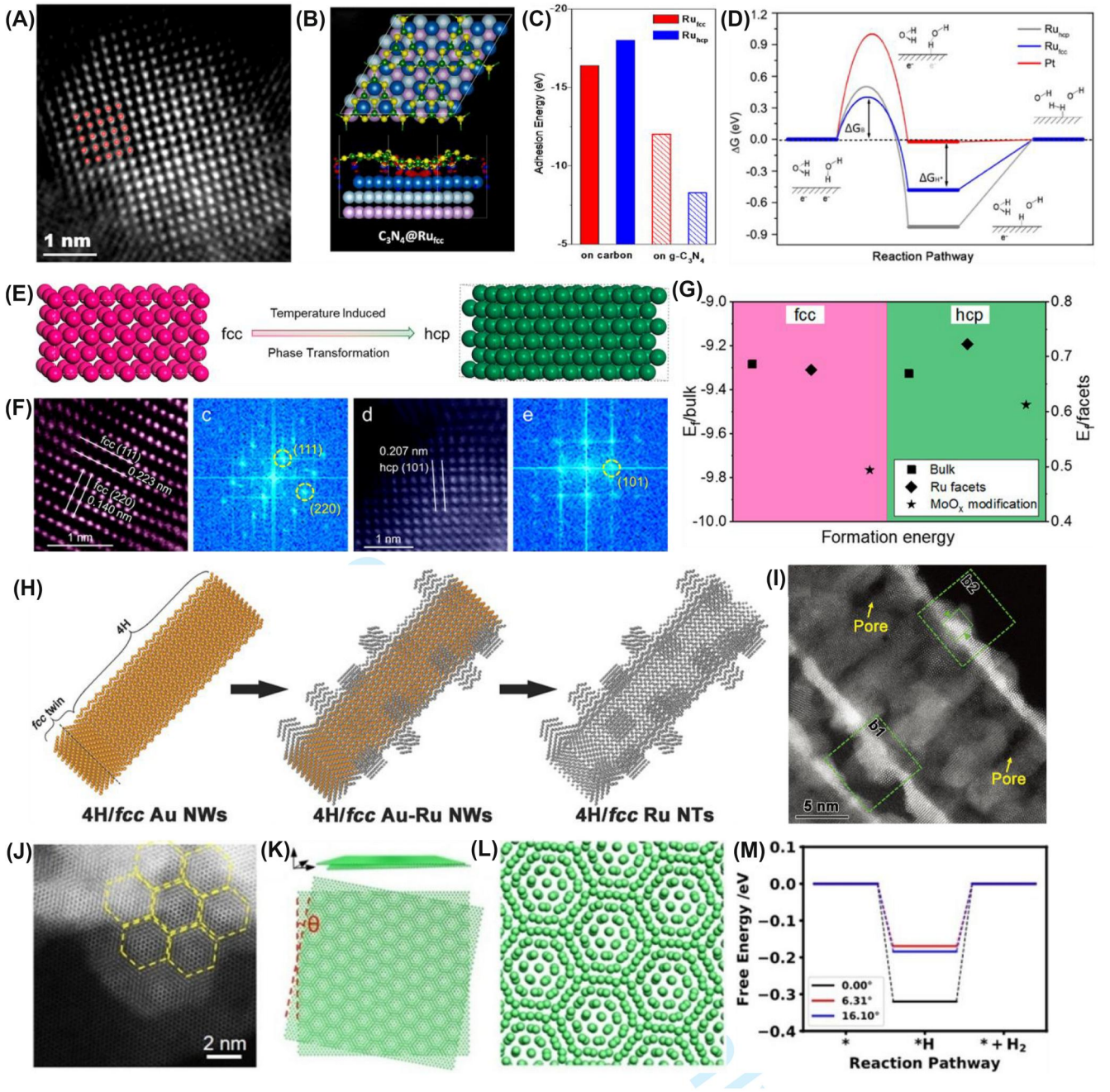

FIGURE 11 (A) HAADF-STEM image of Ru nanoparticle. (B) Atomic configurations (tops) and side views of the electron difference (bottoms) of g-C_3N_4 (2 × 2) and Ru (5 × 5) layers with fcc structure. (C) Comparison of the adhesion energy between carbon/g-C_3N_4 and Ru layers with fcc or hcp structures. (D) Gibbs free energy diagram of HER on different surfaces including reactant initial state, intermediate state, final state, and an additional transition state representing water dissociation.[93] Copyright 2022 American Chemical Society. (E) Crystal models showing the temperature-induced phase transformation. (F) Cs-corrected HAADF STEM images and corresponding FFT of MoO_x-Ru fcc and MoO_x-Ru hcp. (G) Distribution map of formation of energy for metal Ru fcc phase and hcp phase in the condition of bulk, facets (fcc_111 and hcp_101, respectively), and MoO_x modifications.[94] Copyright 2022 American Chemical Society. (H) Schematic illustration of the synthesis of hierarchical 4H/fcc Ru NTs. (I) HAADF-STEM image of a hierarchical 4H/fcc Ru NT.[58] Copyright 2018 Wiley-VCH. (J) HAADF-STEM image with spherical aberration correction of Ru MNSs. (K) 3D and 2D views of the superlattice model. (L) The magnified 2D view of superlattice model. (M) The calculated Gibbs free energies diagram for HER process on Ru MNSs.[59] Copyright 2022 Wiley-VCH. FFT, fast fourier transform; HAADF-STEM, high-angle annular dark field-scanning transmission electron microscopy.

strain to lower the d-band orbit, which weakened the hydrogen adsorption energy and accelerated the H_2 generation rate (Figure 11M). Therefore, it has been certified that phase engineering can optimize crystallinity and surface configuration to design advanced Ru-based catalysts.

2.3 | Local structure alteration

The local structure alteration of nanomaterials, such as lattice strain, structural defects, and local microenvironment can effectively tune the local electronic properties and exposed active sites of nanomaterials to achieve superior catalytic activity toward various applications.[96–98]

2.3.1 | Strain engineering

Strain engineering is induced by the adjusting of Ru–Ru bond length or by the lattice mismatch, which can endow Ru-based catalysts with diverse electronic properties to alter the adsorption capacity of various reaction intermediate species during the alkaline HER.[60,61,98,99] Generally, the strain effect usually exists in the unique core-shell structured catalysts. For instance, Fan et al. fabricated a unique core-shell PdH_x@Ru metallenes by using a seed-mediated growth strategy (Figure 12A).[60] Such a strategy used Pd metallenes as the seed, due to the compressive strain of metallenes compared to bulk. As a result, the prepared PdH_x@Ru metallenes exhibited a 4.5% extensional strained Ru shell, which was induced by the swelled lattice of PdH_x in comparison with Pd. Moreover, the structural stability of PdH_x@Ru metallene was much higher than that of PdH_x metallenes, indicating that PdH_x@Ru metallene was

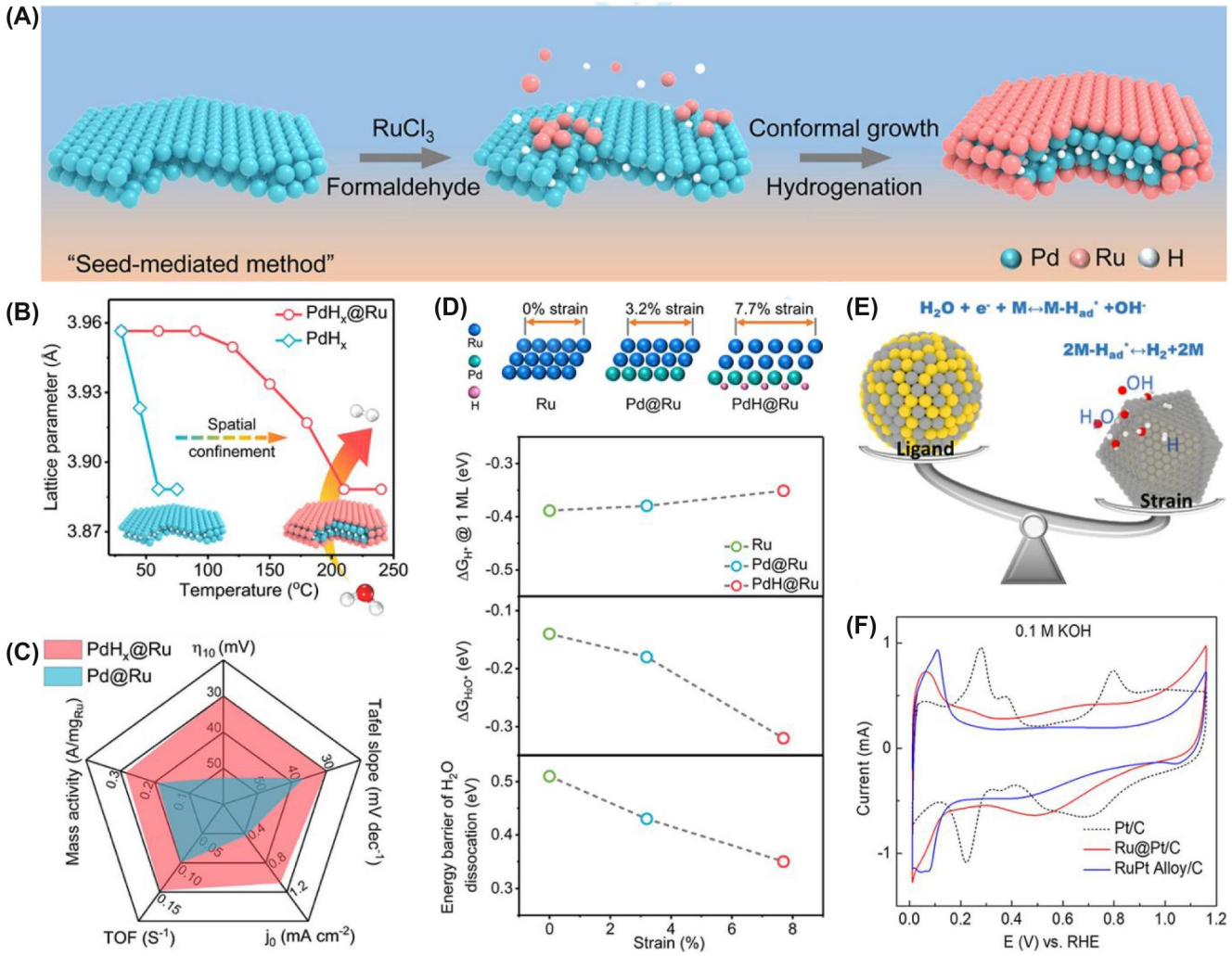

FIGURE 12 (A) Scheme of the growth process of PdH_x@Ru metallenes. (B) The temperature-dependent lattice parameter of PdH_x metallenes and PdH_x@Ru metallenes. (C) Comparison of the HER performance metrics between Pd@Ru metallenes and PdH_x@Ru metallenes. (D) Schematic illustration of the strain variation in the Ru, Pd@Ru, and PdH@Ru surfaces (top) and the ΔG_{H^*} value at 1 ML, the $\Delta G_{H_2O^*}$ value, and the energy barrier of H_2O dissociation as a function of the tensile strain of Ru atoms (bottom).[60] Copyright 2023 American Chemical Society. (E) Schematic illustration of Ru-Pt core-shell (Ru@Pt) and homogeneous alloy (RuPt) model electrocatalysts for the alkaline HER. (F) CVs of various electrocatalysts in 0.1 M KOH showing the H_{UPD} adsorption–desorption peaks.[99] Copyright 2018 American Chemical Society.

more stable (Figure 12B). When acted as a catalyst for the alkaline HER, the PdH_x@Ru metallenes delivered a remarkable activity to reach 10 mA cm^{-2} at 30 mV, superior to the Pt/C benchmark (46 mV) as shown in Figure 12C. Experimental results coupled with DFT calculations presented that the superior activity of PdH_x@Ru metallenes was aroused by the extensional strained Ru shell inherited from the PdH_x core. Such designed strain engineering greatly increased the water adsorption ability, decreased the water cleaving energy, and optimized the hydrogen adsorption energy, thus, accelerating the reaction kinetics (Figure 12D). Moreover, Wang et al. investigated the HER activity in alkaline media and the corresponding mechanism of two types of bimetallic compound, namely, Ru@Pt core-shell and uniform RuPt alloy (Figure 12E).[99] Moreover, the Ru@Pt core-shell catalyst possessed a more greatly compressive strained surface relative to strain-free RuPt alloy, displaying a much higher catalytic activity for the alkaline HER. Experimental measurements showed that the compressive strain in the Ru@Pt catalyst induced an optimized adsorption ability for multiple reaction intermediates during the HER process, hence, enhancing its catalytic activity toward HER in alkaline conditions (Figure 12F).

Except for the core-shell structure, the foreign atom doping can also result in lattice strain. For instance, Li et al. analyzed in detail the relationship between the extendible lattice strain induced by foreign atom doping in CoRu nanoalloys anchored on carbon quantum dots (CoRu/CQDs) and their HER activity in the alkaline electrolyte.[61] Notably, the lattice properties and strain engineering in the CoRu nanoalloys were effectively adjusted by the change of the amount of Ru in the CoRu nanoalloys (Figure 13A). With appropriate lattice strain, the $CoRu_{0.5}$/CQDs showed the best activity (18 mV@10 mA cm^{-2}) toward HER in an alkaline condition relative to other $CoRu_x$/CQDs catalysts (Figure 13B). They found that the lattice strain promoted the d-band orbit approach to the Fermi level, thus, providing optimal hydrogen adsorption ability for H_2 generation. Jiang et al. deposited single Ru atoms on nanoporous MoS_2 (np-MoS_2) with abundant sulfur vacancies (Ru/np-MoS_2) by using a chemical vapor deposition combined with a chemical etching strategy.[62] Impressively, the curvature-caused lattice strain was accurately regulated by the change of the ligament dimension of np-MoS_2 (Figure 13C). The optimal Ru/np-MoS_2 exhibited better activity toward the alkaline HER (30 mV@10 mA cm^{-2}) compared to Ru/Lnp-MoS_2 with less strain (Figure 13D). Combining with the operando XAS, AP-XPS, and DFT calculations, it was confirmed that the strain engineering promoted the aggregation of reaction intermediates (OH^- and H_2O) in sulfur vacancies, which induced the high concentration of reactants in the inner Helmholtz plane to expedite the mass transfer to Ru active sites. Moreover, the bending strain in the Ru/np-MoS_2 further greatly optimized the electronic properties of Ru sites to effectively enhance the water dissociation ability and H_2 generation ability (Figure 13E). Our group designed oxygen vacancies enriched with Ru-zinc solid solution oxide ($Ru_{0.85}Zn_{0.15}O_{2-\delta}$) through a molten salt-assisted strategy (Figure 13F).[63] The optimal $Ru_{0.85}Zn_{0.15}O_{2-\delta}$ reached 10 mA cm^{-2} only using 14 mV for HER in alkaline electrolyte, which is much better than that of Pt/C (32 mV, Figure 13G). Combined with experiments and DFT presented the introduction of Zn atoms and twisted the local structure of $Ru_{0.85}Zn_{0.15}O_{2-\delta}$ to excite the dangling O atoms, which acted as proton receivers. Note that the dangling O atoms are tightly combined with H atoms of the absorbed water molecule to strongly anchor the water molecule, thus, significantly enhancing the catalytic activity for the alkaline HER (Figure 13H,I). However, precisely controlling the strain of the materials to accurately alter their activity is still a hot topic.

2.3.2 | Structural defects

Structural disorder and defect engineering is an effective method to produce active sites in Ru-based catalysts to improve their catalytic activity toward HER in alkaline conditions. Li et al. prepared defect-enriched Ru nanoparticles (DR-Ru) via a galvanic replacement strategy (Figure 14A).[64] The as-prepared DR-Ru arrived at 10 mA cm^{-2} at 28.2 mV for the alkaline HER, which was superior to the commercial Pt/C (61.2 mV). They found that the Ru surface sites with low coordination and the incorporation of lattice oxygen provided an appropriate H_2O/H adsorption energy and an easier water dissociation behavior, which promoted the H_2 production rate in alkaline conditions (Figure 14B,C). Wang et al. have synthesized amorphous $RuTe_2$ porous nanorods with superior catalytic performance under the guidance of DFT.[100] DFT calculations indicated that the increased p-π sensitivity caused by strong p-d transfer could stabilize the distortion strain and increase electronic activities close to the Fermi level by effectively eliminating the crystal–field–splitting effect of Ru (Figure 14D). Accordingly, the homogeneity of charge redistribution capacity between effective orbitals among Ru can be enhanced by the locally distorted Ru–Te lattice (Figure 14E), which not only improves the coupling effect between electron and lattice but also boosts the alkaline HER catalytic performances. In addition, pyrite-type RuS_2 nanoparticles

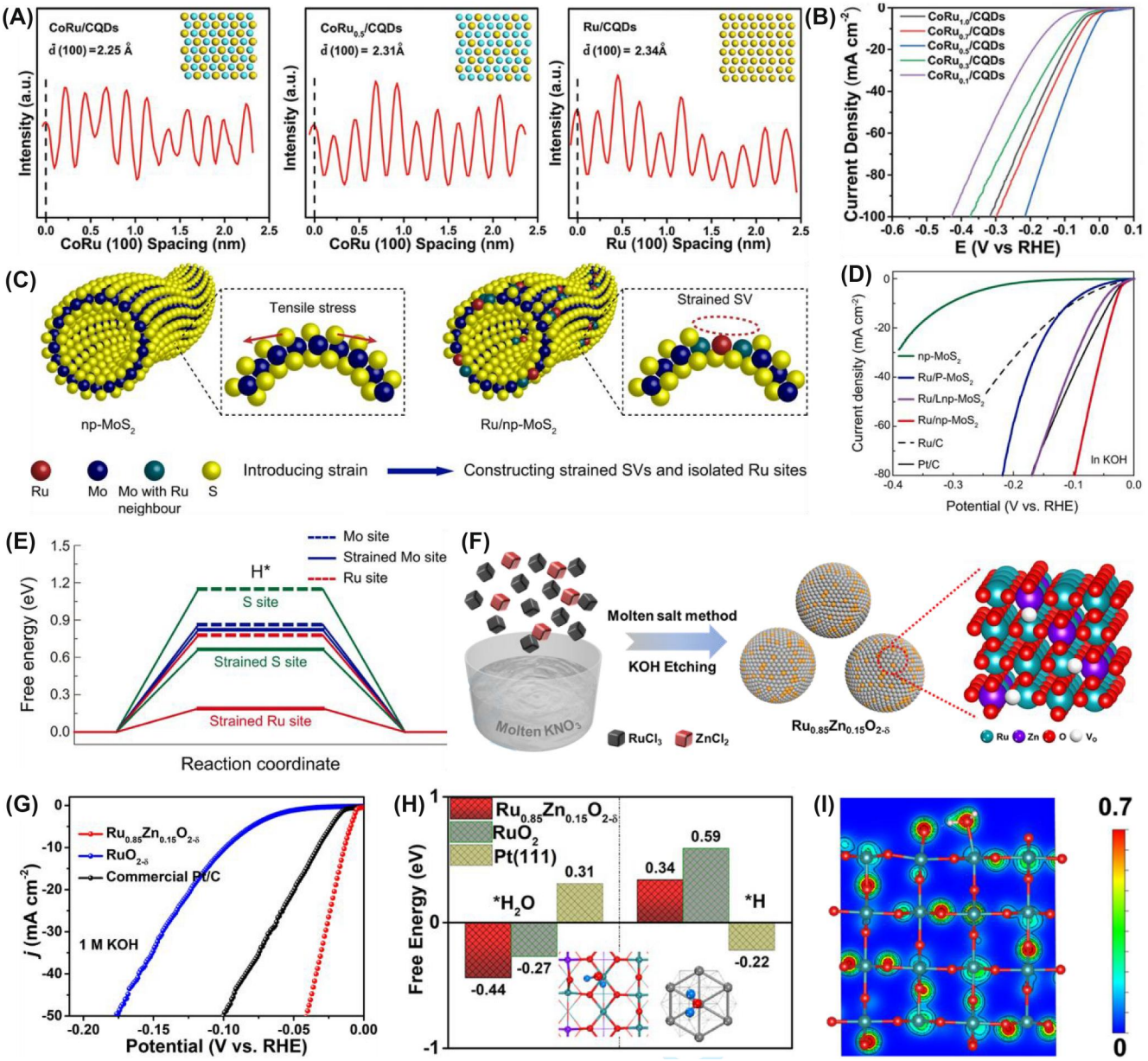

FIGURE 13 (A) Integrated pixel intensities for CoRu/CQDs, $CoRu_{0.5}$/CQDs, and Ru/CQDs lattices. (B) LSV curves for $CoRu_x$/CQDs and Pt/C.[61] Copyright 2020 Wiley-VCH. (C) Illustration of the construction of Ru/np-MoS_2. (D) Polarization curves of Ru/np-MoS_2 as compared with np-MoS_2, Ru/P-MoS_2, Ru/Lnp-MoS_2, Ru/C, and Pt/C. (E) Free energy diagrams for hydrogen adsorption at different sites.[62] Copyright 2021 Springer Nature. (F) Schematic illustration of the synthetic strategy of $Ru_{0.85}Zn_{0.15}O_{2-\delta}$. (G) HER polarization curves of $Ru_{0.85}Zn_{0.15}O_{2-\delta}$ and contrast catalysts in 1 M KOH. (H) The calculated adsorption free energy for H_2O and H adsorbed on $Ru_{0.85}Zn_{0.15}O_{2-\delta}$, RuO_2(110), and Pt(111) surfaces, respectively. (I) The charge density distribution of the H_2O absorbed on the (110) surface of $Ru_{0.85}Zn_{0.15}O_{2-\delta}$.[63] Copyright 2023 Wiley-VCH. LSV, linear sweep voltammetry.

were prepared by a low-temperature sulfuration method (Figure 14F).[65] The disordered structure not only exposed more active sites but also optimized the electronic properties to upshift the Ru d-band center, hence, altering the hydrogen adsorption strength (Figure 14G). Moreover, the newborn sulfide/oxide core/shell structure exhibited a promoted electron transfer, which may be the real active site for improved HER activity.

2.3.3 | Local microenvironment

The local microenvironment surrounding the electrocatalysts has an indelible effect on the electrochemical reaction process but is generally ignored. It also has been demonstrated that the configuration and spatial distribution of micromolecules at the solid–liquid reaction interface are decisive in optimizing the catalytic

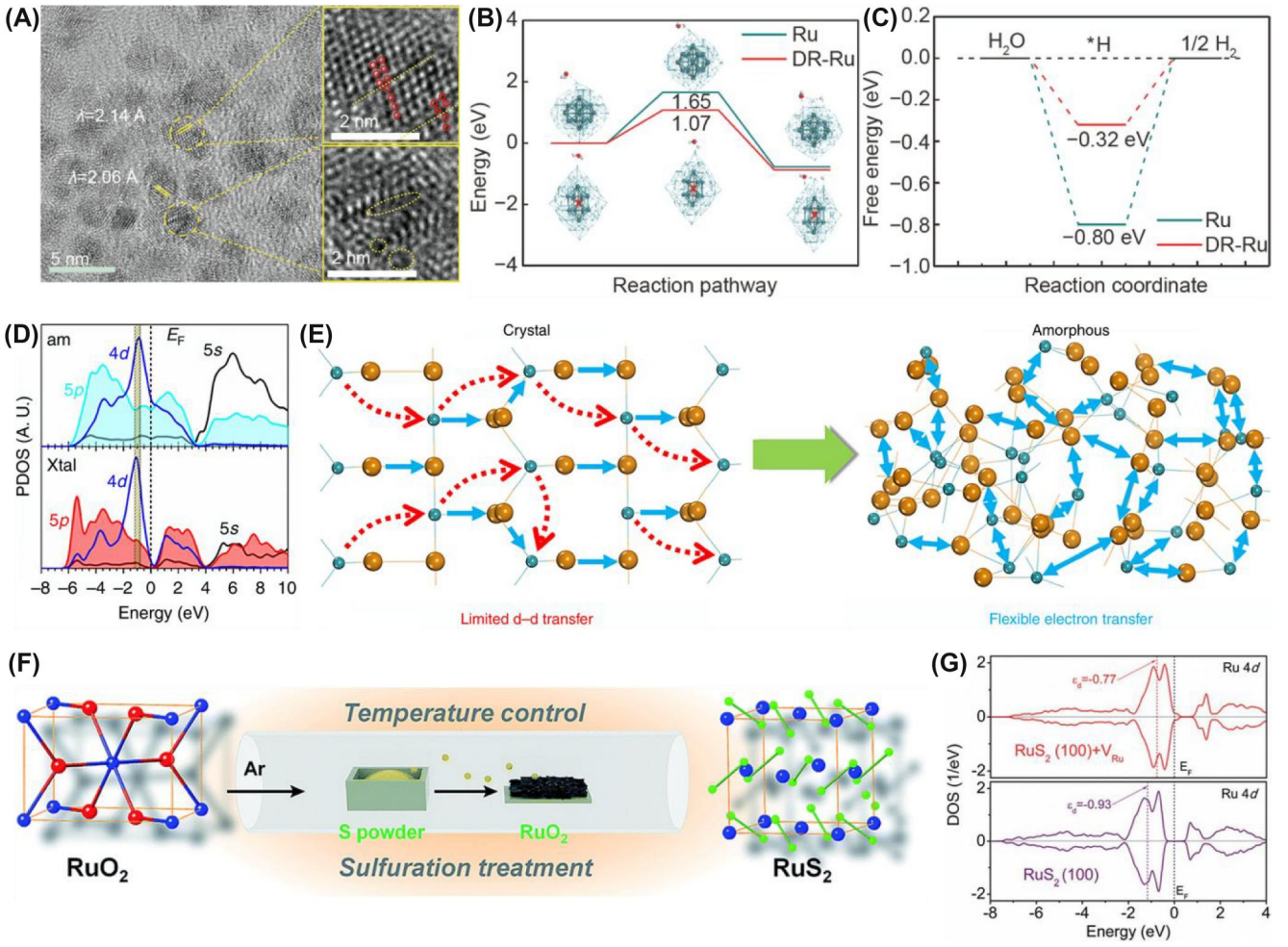

FIGURE 14 (A) HRTEM images of the as-prepared DR-Ru. (B) Calculated reaction barriers for H_2O dissociation on Ru and DR-Ru. (C) Free energy diagram for the HER on Ru and DR-Ru NPs.[64] Copyright 2021 Springer Nature. (D) PDOSs comparison between amorphous and crystalline $RuTe_2$ systems. (E) Schematic diagram of the electronic activity enhancement in amorphous structure.[100] Copyright 2019 Springer Nature. (F) Schematic illustration of the RuS_2 NP synthesis. (G) DOS of Ru 4d on RuS_2 (100) and RuS_2 (100) with V_{Ru}.[65] Copyright 2019 Royal Society of Chemistry. DOS, density of states; HRTEM, high-resolution transmission electron microscopy; PDOS, projected density of states.

performance.[101–103] However, up to now, the studies about the local microenvironment around Ru-related catalysts toward the alkaline HER are still limited. Therefore, exploring effective strategies to alter the local microenvironment of Ru-related materials to increase their catalytic activity is promising and desired.

For example, Gao et al. fabricated a nanocone-convened Ru_3Ni (NA-Ru_3Ni) catalyst via a co-reduction strategy (Figure 15A).[66] Moreover, the obtained NA-Ru_3Ni reached 1000 mA cm^{-2} merely needing an ultra-low overpotential of 168 mV, which is much superior to the Pt/C benchmark (Figure 15B). Finite element simulations combined with experimental tests indicated that the unique structure of NA-Ru_3Ni with specific nanotips induced the formation of a reinforced local electric area, thus, significantly collecting K^+ ions at the interface (Figure 15C,D). The theoretical calculation revealed that the aggregation of hydrated K^+ ion at the local interface resulted in the polarization of the H-OH bond of interfacial H_2O, which provided an easy H_2O dissociation process to contribute to the greatly increased activity for the alkaline HER (Figure 15E–G). Cai et al. constructed double-single Ir/Ru atoms anchored on CoP substrate (IrRu DSACs) by using an impregnation–reduction strategy.[67] The designed IrRu DSACs catalysts promoted the formation of the local electric field with atomical-scale unsymmetric structure, which adjusted the configuration and spatial orientation of adsorbed water, in turn accelerating the reaction kinetics for HER in alkaline conditions (Figure 15H,I). The atomic-scale charge and local electric field distribution surrounding the active sites were intuitively confirmed by the double Cs-corrected scanning transmission electron microscopy (TEM; Figure 15J,K), indicating a high charge density

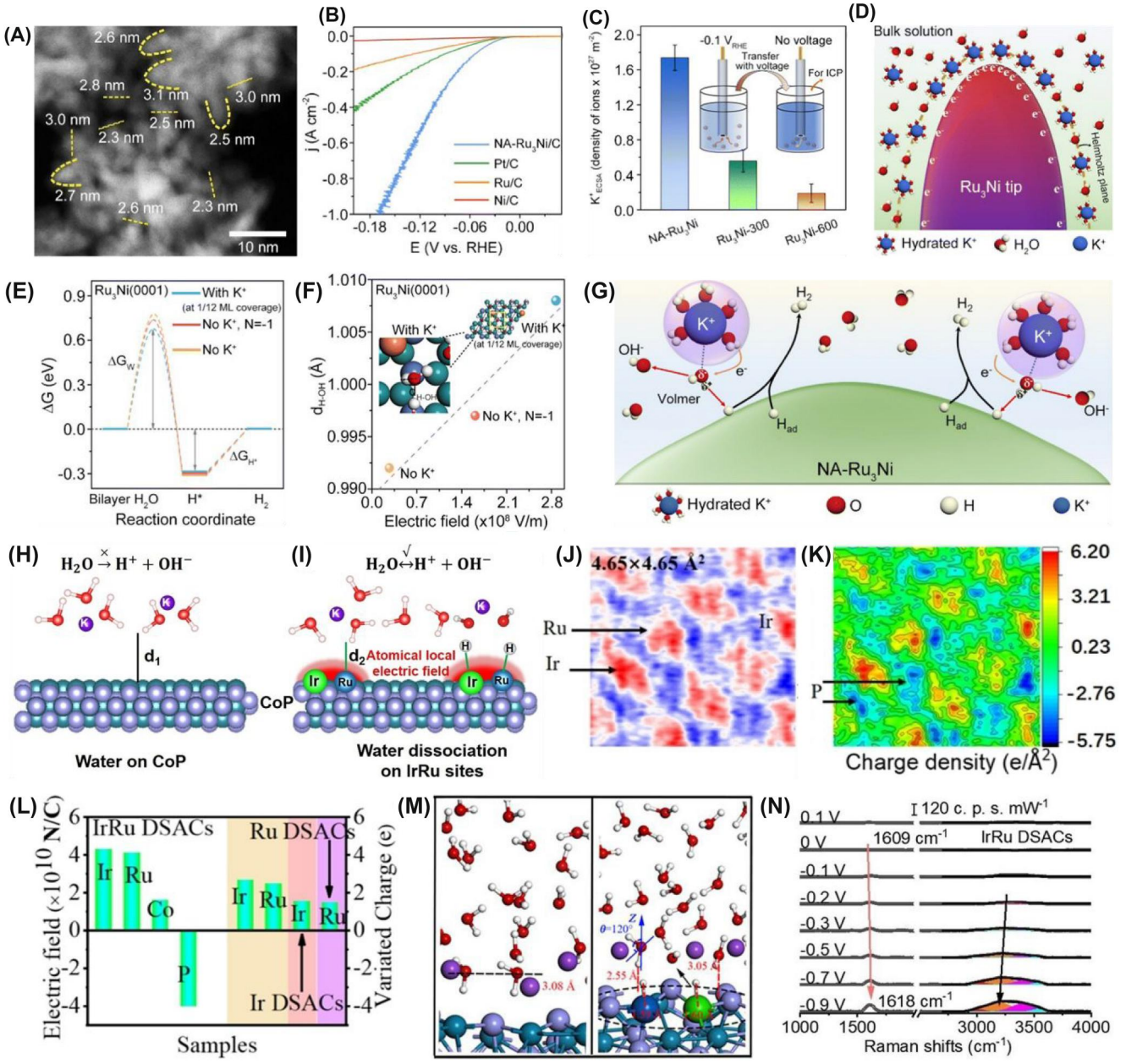

FIGURE 15 (A) HAADF-STEM image of NA-Ru_3Ni. (B) Polarization curves (with iR-correction) were recorded in 1 M KOH solutions at a sweep rate of 5 mV s^{-1}. (C) Comparison of tip-induced K^+ concentration on differently curved Ru_3Ni. The density of K^+ was measured by ICP-MS. The schematic diagram of insertion shows the testing of the adsorbed K^+. (D) Schematic diagram of the interfacial model of NA-Ru_3Ni. (E) Gibbs free energy diagrams of the alkaline HER on different systems. (F) The values of ΔG_{H^*} and ΔG_W on different systems. (G) A schematic diagram showing how K^+ promotes interfacial water dissociation on the NA-Ru_3Ni surface. Schematic diagram of interface H_2O reorientation induced by an atomic electric field.[66] Copyright 2023 Royal Society of Chemistry. H_2O adsorbed on (H) CoP and (I) IrRu DSACs. The selected area integral differential phase contrast-STEM (J), corresponding quantified charge density (K). Total electric field and charge variations of Ir-Ru pairs in IrRu DSACs (L). (M) Interfacial H_2O orientation simulated by ab initio molecular dynamics (AIMD) simulations. (N) The in situ Raman spectra of IrRu DSACs.[67] Copyright 2023 Wiley-VCH. HAADF-STEM, high-angle annular dark field-scanning transmission electron microscopy.

change and electric field intensity of IrRu DSACs (Figure 15L). The ab initio molecular dynamics simulations revealed that the spatial structure of water molecules on the surface of IrRu DSACs was polarized orientation (Figure 15M). In situ Raman measurement verified that the adsorbed construction of water was presented as an unsymmetric H-down coupled with an angle increased by the H-O-H bond, which had a positive effect on the dissociation capacity of water (Figure 15N). Consequently, the IrRu DSACs showcased a remarkable activity for the alkaline HER (10 mV@10 mA cm^{-2}), better than that of Pt/C (31 mV). Note that, up to now, in-

depth research about the local microenvironment of Ru-related electrocatalysts for the alkaline HER is limited and worth our research.

2.4 | Self-optimization

The real active component plays a decisive role in the investigation of the intrinsic catalytic mechanism, while the actual active component relies on whether the catalyst will be reconstructed during the electrocatalytic process.[104–107] The self-reconstruction also occurs for the Ru-based catalysts during the HER process in alkaline conditions.

For example, Zhu et al. homogeneously dispersed Ru-based clusters on the sodium-cobalt oxide layer with the doping of single Ru atoms (Ru/NC) via a cation-exchange reaction strategy.[68] Moreover, the dispersed Ru-based clusters were next to the single Ru atoms. The Ru/NC delivered a Pt-like activity for the alkaline HER (25 mV@10 mA cm^{-2}). Operando XAS results indicated that the prepared Ru/NC compound was the "pre-catalyst" instead of the actual catalytic species. Actually, the Ru hydroxide clusters were effortlessly reduced to metallic Ru clusters during the HER process, thus, revealing that both the single Ru atoms and Ru clusters acted as active sites for the alkaline HER (Figure 16A), which was also confirmed by further theoretical calculations. Zhang et al. reported a monocrystalline Sr_2RuO_4 bulk (Figure 16B),[69] synthesized by using a floating-zone strategy, which acted as the alkaline HER catalyst. Such catalysts arrived at 1000 mA cm^{-2} only requiring 278 mV and also displayed superior stability over 56 days with successive working under an ampere current density and then at high working operating temperatures up to 70°C (Figure 16C). They found that there was surface reconstruction during the electrocatalytic process with the in situ generation of ferromagnetic Ru nanoclusters at the Sr_2RuO_4 bulk surface through elemental mapping, TEM, and XPS (Figure 16D). Such self-reconstruction improved the charge transfer ability and wettability of the monocrystalline catalyst, enabling the fast H_2 production behavior even under ampere current densities (Figure 16E). Pang et al. synthesized PtRu alloy nanoparticles anchored on surface-

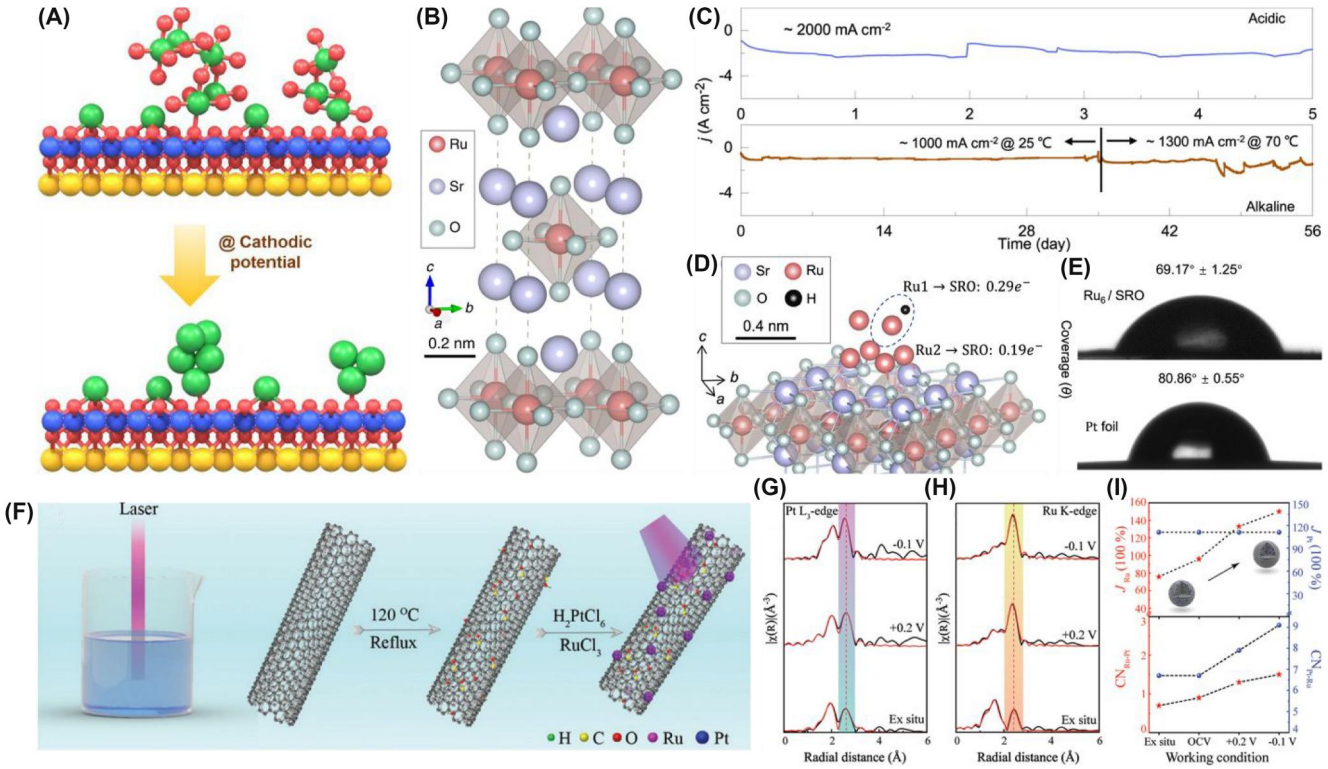

FIGURE 16 (A) Schematic model of the structural transformation in Ru/NC toward HER.[68] Copyright 2023 Wiley-VCH. (B) Three-dimensional crystal structure of layered SRO crystal. (C) Long-term stability test of the SRO catalyst in acidic and alkaline conditions at room temperature and 70 °C (1 M KOH). (D) Optimized hydrogen adsorption of H atom at the surface of Ru_6/SRO.[69] Copyright 2022 Springer Nature. (E) Water contact angles of Ru_6/SRO and Pt foil catalysts. (F) Schematic illustration of the manufacture of the PtRu/mCNTs catalyst. Least-squares curve-fitting analysis of operando EXAFS spectra at the Pt L_3-edge (G) and Ru K-edge (H). (I) The fitted structural parameters of PtRu/mCNTs and alloying degree under working conditions.[70] Copyright 2022 Royal Society of Chemistry. SRO, Sr_2RuO_4.

embellished carbon nanotube (PtRu/mCNTs) by using laser irradiation in liquid strategy (Figure 16F).[70] The obtained PtRu/mCNTs exhibited a small overpotential of 15 mV to reach 10 mA cm^{-2} in alkaline electrolyte for HER, which was superior to the commercial Pt/C (39 mV). Operando XAS results confirmed that there was a surface reconstruction of PtRu nanoparticles during the HER process. Moreover, Pt atoms were inclined to move from the surface to the interior of PtRu nanoparticles, increasing the alloying degree between Pt and Ru atoms (Figure 16G–I). Such self-optimization of PtRu/mCNTs greatly regulated both their geometric and electronic structure, enabling a remarkable activity toward the alkaline HER. Therefore, it is very important that the self-optimization process and identification of the real active sites need to be investigated in detail to understand the reaction essence of Ru-related electrocatalysts for the alkaline HER.

3 | CONCLUSIONS AND PERSPECTIVES

Various Ru-related catalysts toward the alkaline HER have been explored with the step forward of theoretical simulation techniques and material engineering techniques. The above-involved Ru-based HER catalysts include Ru-based alloys, Ru-based MOFs, Ru-based sulfides, and Ru-based oxides, all of which possess enough exposed active sites, anchoring preference effect of reaction intermediate species during the alkaline HER process. Moreover, the above-summarized effective material engineering methods are designed either to optimize the interaction between the catalytic species and specific reaction intermediate species or to reduce the reaction energy barrier of the overall HER process. Of note, various material engineering strategies may not have any preference for the different kinds of Ru-related materials. For example, although the discussion of the aforementioned metal element engineering mainly focuses on Ru-based alloys, this strategy can also be appropriate for Ru-based MOFs and Ru-based metal oxides, etc.[54,63] In addition, these strategies may be also used to design advanced catalysts toward other electrocatalytic reactions. Furthermore, to profoundly understand and control the design of Ru-related electrocatalysts toward the alkaline HER, several challenges and opportunities should be a concern as illustrated in Figure 17.

3.1 | Development of practical hydrogen evolution electrocatalysts

A major remaining issue is that the mass loading of Ru in mostly reported Ru-based catalysts is still relatively high,

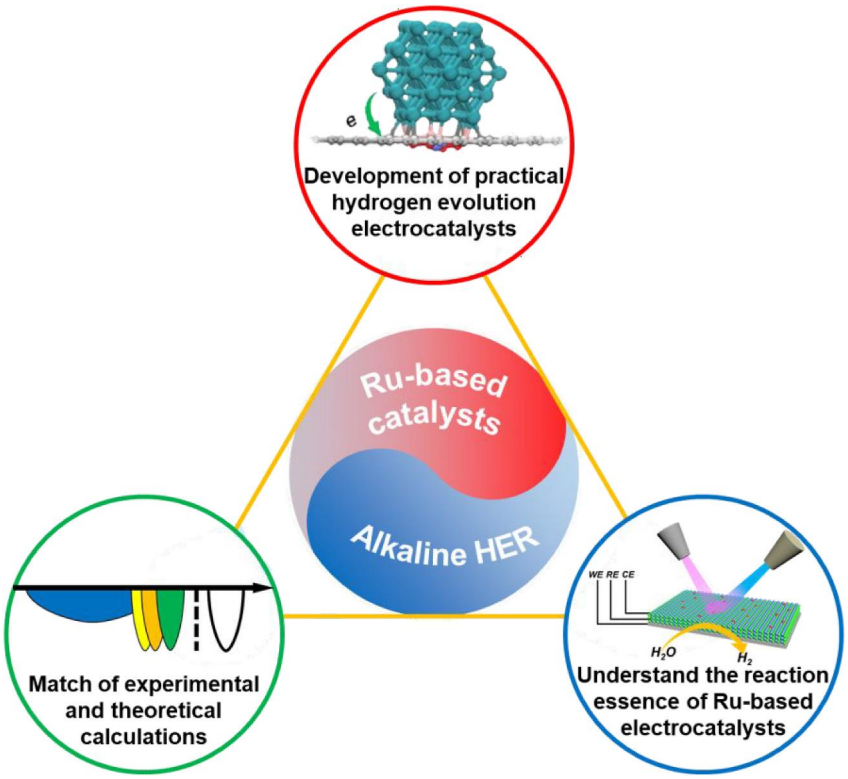

FIGURE 17 Summary of challenges and future perspectives to design advanced Ru-based catalysts.

relative to the unique properties of the noble Ru metal. Such results will extremely hinder the mass production of Ru-based catalysts for the alkaline HER with low cost. For the future development of highly active Ru-related HER electrocatalysts with low dosages of Ru, firmly dispersing sub-nanometer Ru clusters on the substrates can perhaps be an effective and promising method. It has been demonstrated that sub-nanometer Ru clusters are more active for the alkaline HER relative to Ru nanoparticles and single atoms. The supported Ru clusters cannot merely increase the availability efficiency of Ru atoms compared to Ru nanoparticles but also create a more versatile interfacial local coordination environment than those of either Ru single-atoms or nanoparticles. Furthermore, the specific geometric nanostructure of supported Ru cluster catalysts, to some extent, can provide the maximum utilization of metal atoms around the metal–support interface, and the spontaneously formed EMSI can also contribute to enhancing both the activity and stability of Ru-related catalysts toward the alkaline HER.

3.2 | Understanding the reaction essence of Ru-based electrocatalysts

The real active sites and deactivation phenomenon need to be investigated in detail by more advanced characterization techniques, such as in situ scanning electrochemical microscopy, X-ray and vibrational spectroscopies, and so on. Meanwhile, the local microenvironments (such as local ionic concentration, electric field, pH, and electric double layer, etc.) and the dynamic conversion of catalysts surface play a decisive role in the determinant of actual active species and deactivation factor, which should be taken seriously in future research.

3.3 | Match of experimental and theoretical calculations

Last but not the least, more comprehensive theoretical calculations need to be explored and used for Ru-based HER catalysts, owing to most of the reported simulated results based on the overlook of actual experimental conditions, such as pH, electric field, solvation effect, etc. Accordingly, the theoretical calculations should be closely combined with the experimental data, especially the in situ characterization data, which would preferably uncover the actual H_2 generation process. Moreover, high-throughput theoretical calculations are suggested to screen and design advanced Ru-based catalysts for the alkaline HER.

ACKNOWLEDGMENTS

We gratefully acknowledge the financial support from the Natural Science Foundation of Shandong Province of China (ZR2022QB100), and Science Foundation of Qingdao University of Science and Technology (12030430010936).

CONFLICT OF INTEREST STATEMENT

The authors declare no competing interests.

DATA AVAILABILITY STATEMENT

The data that support the findings of this study are available from the corresponding author upon reasonable request.

ORCID

Xien Liu https://orcid.org/0000-0002-4947-0631

REFERENCES

1. Zeng K, Zhang D. Recent progress in alkaline water electrolysis for hydrogen production and applications. *Prog Energy Combust Sci*. 2010;36(3):307-326.
2. Zou C, Zhao Q, Zhang G, Xiong B. Energy revolution: from a fossil energy era to a new energy era. *Nat Gas Ind*. 2016;3(1):1-11.
3. Olabi A, Abdelkareem MA. Renewable energy and climate change. *Renew Sustain Energy Rev*. 2022;158:112111.
4. Abdalla AM, Hossain S, Nisfindy OB, Azad AT, Dawood M, Azad AK. Hydrogen production, storage, transportation and key challenges with applications: a review. *Energy Convers Manag*. 2018;165:602-627.
5. Sharma S, Ghoshal SK. Hydrogen the future transportation fuel: from production to applications. *Renew Sustain Energy Rev*. 2015;43:1151-1158.
6. Zheng D, Yu L, Liu W, et al. Structural advantages and enhancement strategies of heterostructure water-splitting electrocatalysts. *Cell Rep Phys Sci*. 2021;2(6):100443.
7. Zhang Y, Li Z, Hou L, Liu X. Thermal shrinkage engineering enables electrocatalysts for stable hydrogen evolution at 2000 mA cm^{-2}. *Adv Funct Mater*. 2023;33(16):2213976.
8. Li L, Wang P, Shao Q, Huang X. Metallic nanostructures with low dimensionality for electrochemical water splitting. *Chem Soc Rev*. 2020;49(10):3072-3106.
9. Wang X, Zheng Y, Sheng W, Xu ZJ, Jaroniec M, Qiao S-Z. Strategies for design of electrocatalysts for hydrogen evolution under alkaline conditions. *Mater Today*. 2020;36:125-138.
10. Zheng Y, Jiao Y, Vasileff A, Qiao SZ. The hydrogen evolution reaction in alkaline solution: from theory, single crystal models, to practical electrocatalysts. *Angew Chem Int Ed*. 2018;57(26):7568-7579.
11. Wei J, Zhou M, Long A, et al. Heterostructured electrocatalysts for hydrogen evolution reaction under alkaline conditions. *Nano-Micro Lett*. 2018;10(4):75.
12. Zhang L, Lang Z, Wang Y, et al. Cable-like Ru/WNO@C nanowires for simultaneous high-efficiency hydrogen evolution and low-energy consumption chlor-alkali electrolysis. *Energy Environ Sci*. 2019;12(8):2569-2580.

13. Liu Y, Li GD, Yuan L, et al. Carbon-protected bimetallic carbide nanoparticles for a highly efficient alkaline hydrogen evolution reaction. *Nanoscale*. 2015;7(7):3130-3136.
14. Zhang LN, Li R, Zang HY, et al. Advanced hydrogen evolution electrocatalysts promising sustainable hydrogen and chlor-alkali co-production. *Energy Environ Sci*. 2021;14(12):6191-6210.
15. Schmidt TJ, Ross PN, Markovic NM. Temperature dependent surface electrochemistry on Pt single crystals in alkaline electrolytes. *J Electroanal Chem*. 2002;524(2):252-260.
16. Markovic NM, Schmidt TJ, Grgur BN, Gasteiger HA, Behm RJ, Ross PN. Effect of temperature on surface processes at the Pt(111)–liquid interface: hydrogen adsorption, oxide formation, and CO oxidation. *J Phys Chem B*. 1999;103(40):8568-8577.
17. Gao Q, Zhang W, Shi Z, Yang L, Tang Y. Structural design and electronic modulation of transition-metal-carbide electrocatalysts toward efficient hydrogen evolution. *Adv Mater*. 2019;31(2):1802880.
18. Zhu J, Hu L, Zhao P, Lee L, Wong KY. Recent advances in electrocatalytic hydrogen evolution using nanoparticles. *Chem Rev*. 2020;120(2):851-918.
19. Zhai W, Ma Y, Chen D, Ho JC, Dai Z, Qu Y. Recent progress on the long-term stability of hydrogen evolution reaction electrocatalysts. *InfoMat*. 2022;4(9):e12357.
20. Subbaraman R, Tripkovic D, Strmcnik D, et al. Enhancing hydrogen evolution activity in water splitting by tailoring Li^+-$Ni(OH)_2$-Pt interfaces. *Science*. 2012;334(6060):1256-1260.
21. Yu FY, Lang ZL, Yin LY, et al. Pt-O bond as an active site superior to Pt^0 in hydrogen evolution reaction. *Nat Commun*. 2020;11(1):490.
22. Wang X, Zhao L, Li X, et al. Atomic-precision Pt_6 nanoclusters for enhanced hydrogen electro-oxidation. *Nat Commun*. 2022;13(1):1596.
23. Pei Y, Moghadam B, Zhang X, Li Z, Wang J. Interface catalysis by Pt nanocluster@Ni_3N for bifunctional hydrogen evolution and oxygen evolution. *Mater Chem Front*. 2020;4(9):2665-2672.
24. Qiao Z, Wang C, Zeng Y, Spendelow JS, Wu G. Advanced nanocarbons for enhanced performance and durability of platinum catalysts in proton exchange membrane fuel cells. *Small*. 2021;17(48):2006805.
25. Zhang Z, Liu H, Ni L, Zhao Z, Li H. Scalable synthesis of hcp ruthenium-molybdenum nanoalloy as a robust bifunctional electrocatalyst for hydrogen evolution/oxidation. *J Energy Chem*. 2022;72:176-185.
26. Xue Y, Shi L, Liu X, et al. A highly-active, stable and low-cost platinum-free anode catalyst based on RuNi for hydroxide exchange membrane fuel cells. *Nat Commun*. 2020;11(1):5651.
27. Li C, Jang H, Liu S, et al. P and Mo dual doped Ru ultrasmall nanoclusters embedded in P-doped porous carbon toward efficient hydrogen evolution reaction. *Adv Energy Mater*. 2022;12(23):2200029.
28. He Q, Tian D, Jiang H, Cao D, Song L. Achieving efficient alkaline hydrogen evolution reaction over a Ni_5P_4 catalyst incorporating single-atomic Ru sites. *Adv Mater*. 2020;32(11):1906972.
29. Zhang S, Li J, Wang E. Recent progress of ruthenium-based nanomaterials for electrochemical hydrogen evolution. *Chemelectrochem*. 2020;7(22):4526-4534.
30. Bae S-Y, Mahmood J, Jeon I-Y, Baek J-B. Recent advances in ruthenium-based electrocatalysts for the hydrogen evolution reaction. *Nanoscale Horiz*. 2020;5(1):43-56.
31. Chen C, Wu D, Li Z, et al. Ruthenium-based single-atom alloy with high electrocatalytic activity for hydrogen evolution. *Adv Energy Mater*. 2019;9(20):1803913.
32. Mu X, Gu J, Feng F, et al. RuRh bimetallene nanoring as high-efficiency pH-universal catalyst for hydrogen evolution reaction. *Adv Sci*. 2021;8(2):2002341.
33. Liu Y, Li X, Zhang Q, et al. A general route to prepare low-ruthenium-content bimetallic electrocatalysts for pH-universal hydrogen evolution reaction by using carbon quantum dots. *Angew Chem Int Ed*. 2020;59(4):1718-1726.
34. Zhao X, Wu G, Zheng X, et al. A double atomic-tuned RuBi SAA/Bi@OG nanostructure with optimum charge redistribution for efficient hydrogen evolution. *Angew Chem Int Ed*. 2023;62(12):e202300879.
35. Cai C, Liu K, Zhu Y, et al. Optimizing hydrogen binding on Ru sites with RuCo alloy nanosheets for efficient alkaline hydrogen evolution. *Angew Chem Int Ed*. 2022;61(4):e202113664.
36. Liu G, Zhou W, Chen B, et al. Synthesis of RuNi alloy nanostructures composed of multilayered nanosheets for highly efficient electrocatalytic hydrogen evolution. *Nano Energy*. 2019;66:104173.
37. Yao Q, Huang B, Zhang N, Sun M, Shao Q, Huang X. Channel-rich RuCu nanosheets for pH-universal overall water splitting electrocatalysis. *Angew Chem Int Ed*. 2019;58(39):13983-13988.
38. Shen S, Hu Z, Zhang H, et al. Highly active Si sites enabled by negative valent Ru for electrocatalytic hydrogen evolution in LaRuSi. *Angew Chem Int Ed*. 2022;134(32):e202206460.
39. Hao J, Zhuang Z, Cao K, et al. Unraveling the electronegativity-dominated intermediate adsorption on high-entropy alloy electrocatalysts. *Nat Commun*. 2022;13(1):2662.
40. Zhao Y, Wang X, Cheng G, Luo W. Phosphorus-induced activation of ruthenium for boosting hydrogen oxidation and evolution electrocatalysis. *ACS Catal*. 2020;10(20):11751-11757.
41. Liu X, Liu F, Yu J, Xiong G, Zhou W. Charge redistribution caused by S,P synergistically active Ru endows an ultrahigh hydrogen evolution activity of S-doped RuP embedded in N,P,S-doped carbon. *Adv Sci*. 2020;7(17):2001526.
42. Tu K, Tranca D, Hernández FR, et al. A novel heterostructure based on RuMo nanoalloys and N-doped carbon as an efficient electrocatalyst for the hydrogen evolution reaction. *Adv Mater*. 2020;32(46):2005433.
43. Chen D, Yu R, Lu R, et al. Tunable Ru-Ru_2P heterostructures with charge redistribution for efficient pH-universal hydrogen evolution. *InfoMat*. 2022;4(5):e12287.
44. Jiang X, Jang H, Liu S, et al. The heterostructure of Ru_2P/-WO_3/NPC synergistically promotes H_2O dissociation for improved hydrogen evolution. *Angew Chem Int Ed*. 2021;60(8):4110-4116.
45. Salah A, Zhang L, Tan H, et al. Advanced Ru/Ni/WC@NPC multi-interfacial electrocatalyst for efficient sustainable hydrogen and chlor-alkali co-production. *Adv Energy Mater*. 2022;12(21):2200332.

46. Li F, Han G, Noh H-J, Ahmad I, Jeon I-Y, Baek J-B. Mechanochemically assisted synthesis of a Ru catalyst for hydrogen evolution with performance superior to Pt in both acidic and alkaline media. *Adv Mater*. 2018;30(44):1803676.
47. Ye S, Luo F, Xu T, et al. Boosting the alkaline hydrogen evolution of Ru nanoclusters anchored on B/N–doped graphene by accelerating water dissociation. *Nano Energy*. 2020; 68:104301.
48. Su P, Pei W, Wang X, et al. Exceptional electrochemical HER performance with enhanced electron transfer between Ru nanoparticles and single atoms dispersed on a carbon substrate. *Angew Chem Int Ed*. 2021;60(29):16044-16050.
49. Li C, Kim SH, Lim HY, et al. Self-accommodation induced electronic metal-support interaction on ruthenium site for alkaline hydrogen evolution reaction. *Adv Mater*. 2023; 35(21):2301369.
50. Chen L, Wang S, Zhang P, et al. Ru nanoparticles supported on partially reduced TiO_2 as highly efficient catalyst for hydrogen evolution. *Nano Energy*. 2021;88:106211.
51. Zhou S, Jang H, Qin Q, et al. Boosting hydrogen evolution reaction by phase engineering and phosphorus doping on Ru/P-TiO_2. *Angew Chem Int Ed*. 2022;61(47):e202212196.
52. Li G, Jang H, Liu S, et al. The synergistic effect of Hf-O-Ru bonds and oxygen vacancies in Ru/HfO_2 for enhanced hydrogen evolution. *Nat Commun*. 2022;13(1):1270.
53. Sun Y, Xue Z, Liu Q, et al. Modulating electronic structure of metal-organic frameworks by introducing atomically dispersed Ru for efficient hydrogen evolution. *Nat Commun*. 2021;12(1):1369.
54. Peng S, Deng L-M, Hu F-X, et al. Electronic modulation caused by interfacial Ni-O-M (M=Ru, Ir, Pd) bonding for accelerating hydrogen evolution kinetics. *Angew Chem Int Ed*. 2021;60(41):22276-22282.
55. Zhang L, Jang H, Wang Y, et al. Exploring the dominant role of atomic- and nano-ruthenium as active sites for hydrogen evolution reaction in both acidic and alkaline media. *Adv Sci*. 2021;8(15):2004516.
56. Hu Q, Gao K, Wang X, et al. Subnanometric Ru clusters with upshifted D band center improve performance for alkaline hydrogen evolution reaction. *Nat Commun*. 2022;13(1):3958.
57. Liang Q, Li Q, Xie L, et al. Superassembly of surface-enriched Ru nanoclusters from trapping–bonding strategy for efficient hydrogen evolution. *ACS Nano*. 2022;16(5):7993-8004.
58. Lu Q, Wang AL, Cheng H, et al. Synthesis of hierarchical 4H/fcc Ru nanotubes for highly efficient hydrogen evolution in alkaline media. *Small*. 2018;14(30):1801090.
59. Zhang J, Mao X, Wang S, et al. Superlattice in a Ru superstructure for enhancing hydrogen evolution. *Angew Chem Int Ed*. 2022;61(14):e202116867.
60. Fan J, Feng Z, Mu Y, et al. Spatially confined PdH_x metallenes by tensile strained atomic Ru layers for efficient hydrogen evolution. *J Am Chem Soc*. 2023;145(10):5710-5717.
61. Li W, Zhao Y, Liu Y, et al. Exploiting Ru-induced lattice strain in CoRu nanoalloys for robust bifunctional hydrogen production. *Angew Chem Int Ed*. 2020;60(6):3290-3298.
62. Jiang K, Luo M, Liu Z, et al. Rational strain engineering of single-atom ruthenium on nanoporous MoS_2 for highly efficient hydrogen evolution. *Nat Commun*. 2021;12(1): 1687.
63. Hou L, Li Z, Jang H, et al. Electronic and lattice engineering of ruthenium oxide towards highly active and stable water splitting. *Adv Energy Mater*. 2023;13(22):2300177.
64. Li Y, He J, Cheng W, et al. High mass-specific reactivity of a defect-enriched Ru electrocatalyst for hydrogen evolution in harsh alkaline and acidic media. *Sci China Mater*. 2021; 64(10):2467-2476.
65. Zhu Y, Tahini H, Wang Y, et al. Pyrite-type ruthenium disulfide with tunable disorder and defects enables ultra-efficient overall water splitting. *J Mater Chem A*. 2019;7(23): 14222-14232.
66. Gao L, Bao F, Tan X, et al. Engineering a local potassium cation concentrated microenvironment toward the ampere-level current density hydrogen evolution reaction. *Energy Environ Sci*. 2023;16(1):285-294.
67. Cai C, Liu K, Zhang L, et al. Atomically local electric field induced interface water reorientation for alkaline hydrogen evolution reaction. *Angew Chem Int Ed*. 2023;62(26): e202300873.
68. Zhu Y, Fan K, Hsu C-S, et al. Supported ruthenium single-atom and clustered catalysts outperform benchmark Pt for alkaline hydrogen evolution. *Adv Mater*. 2023;35(35):2301133.
69. Zhang Y, Arpino K, Yang Q, et al. Observation of a robust and active catalyst for hydrogen evolution under high current densities. *Nat Commun*. 2022;13(1):7784.
70. Pang B, Liu X, Liu T, et al. Laser-assisted high-performance PtRu alloy for pH-universal hydrogen evolution. *Energy Environ Sci*. 2022;15(1):102-108.
71. Yang J, Li W, Wang D, Li Y. Electronic metal-support interaction of single-atom catalysts and applications in electrocatalysis. *Adv Mater*. 2020;32(49):2003300.
72. Rong C, Shen X, Wang Y, et al. Electronic structure engineering of single-atom Ru sites via Co-N_4 sites for bifunctional pH-universal water splitting. *Adv Mater*. 2022;34(21):2110103.
73. María E, Jensen KD, Jensen AW. Recent advances in bimetallic electrocatalysts for oxygen reduction: design principles, structure-function relations and active phase elucidation. *Curr Opin Electrochem*. 2018;8:135.
74. Qiao Y, Yuan P, Pao C, et al. Boron-rich environment boosting ruthenium boride on B, N doped carbon outperforms platinum for hydrogen evolution reaction in a universal pH range. *Nano Energy*. 2020;75:104881.
75. Shi Y, Ma ZR, Xiao YY, et al. Electronic metal–support interaction modulates single-atom platinum catalysis for hydrogen evolution reaction. *Nat Commun*. 2021;12(1):3021.
76. Wang D, Yang J, Li WH, et al. The electronic metal–support interaction directing the design of single atomic site catalysts: achieving high efficiency towards hydrogen evolution. *Angew Chem Int Ed*. 2021;60(35):19085-19091.
77. He H, Chen J, Zhang D, et al. Modulating the electrocatalytic performance of palladium with the electronic metal–support interaction: a case study on oxygen evolution reaction. *ACS Catal*. 2018;8(7):6617-6626.
78. Hwang J, Rao RR, Giordano L, Katayama Y, Yu Y, Shao-Horn Y. Perovskites in catalysis and electrocatalysis. *Science*. 2017;358(6364):751-756.
79. Lang R, Du X, Huang Y, et al. Single-atom catalysts based on the metal–oxide interaction. *Chem Rev*. 2020;120(21): 11986-12043.

80. Xue Y, Sun S, Wang Q, Dong Z, Liu Z. Transition metal oxide-based oxygen reduction reaction electrocatalysts for energy conversion systems with aqueous electrolytes. *J Mater Chem A*. 2018;6(23):10595-10626.
81. Li C, Jang H, Kim MG, Hou L, Liu X, Cho J. Ru-incorporated oxygen-vacancy-enriched MoO_2 electrocatalysts for hydrogen evolution reaction. *Appl Catal, B*. 2022;307:121204.
82. Xu J, Chen C, Kong X. Ru-O-Cu center constructed by catalytic growth of Ru for efficient hydrogen evolution. *Nano Energy*. 2023;111:108403.
83. Zhang J, Chen G, Liu Q, et al. Competitive adsorption: reducing the poisoning effect of adsorbed hydroxyl on Ru single-atom site with SnO_2 for efficient hydrogen evolution. *Angew Chem Int Ed*. 2022;61(39):e202209486.
84. Zhao M, Yuan K, Wang Y, et al. Metal–organic frameworks as selectivity regulators for hydrogenation reactions. *Nature*. 2016;539(7627):76-80.
85. Shen J-Q, Liao PQ, Zhou DD, et al. Modular and stepwise synthesis of a hybrid metal–organic framework for efficient electrocatalytic oxygen evolution. *J Am Chem Soc*. 2017;139(5):1778-1781.
86. Fang R, Dhakshinamoorthy A, Li Y, García H. Metal organic frameworks for biomass conversion. *Chem Soc Rev*. 2020;49(11):3638-3687.
87. Chen Y, Lai Z, Zhang X, et al. Phase engineering of nanomaterials. *Nat Rev Chem*. 2020;4(5):243-256.
88. Zhang B, Chen Y, Wang J, Pan H, Sun W. Supported subnanometer clusters for electrocatalysis applications. *Adv Funct Mater*. 2022;32(24):2202227.
89. Li W, Liu Y, Wu M, et al. Carbon-quantum-dots-loaded ruthenium nanoparticles as an efficient electrocatalyst for hydrogen production in alkaline media. *Adv Mater*. 2018;30(31):1800676.
90. Yu J, He Q, Yang G, Zhou W, Shao Z, Ni M. Recent advances and prospective in ruthenium-based materials for electrochemical water splitting. *ACS Catal*. 2019;9(11):9973-10011.
91. Zhao M, Xia Y. Crystal-phase and surface-structure engineering of ruthenium nanocrystals. *Nat Rev Mater*. 2020;5(6):440-459.
92. Zhao M, Hood ZD, Vara M, Gilroy K, Chi M, Xia Y. Ruthenium nanoframes in the face-centered cubic phase: facile synthesis and their enhanced catalytic performance. *ACS Nano*. 2019;13(6):7241-7251.
93. Zheng Y, Jiao Y, Zhu Y, et al. High electrocatalytic hydrogen evolution activity of an anomalous ruthenium catalyst. *J Am Chem Soc*. 2016;138(49):16174-16181.
94. Li L, Liu C, Liu S, et al. Phase engineering of a ruthenium nanostructure toward high-performance bifunctional hydrogen catalysis. *ACS Nano*. 2022;16(9):14885-14894.
95. Gao K, Wang Y, Wang Z, et al. Ru nanodendrites composed of ultrathin fcc/hcp nanoblades for the hydrogen evolution reaction in alkaline solutions. *Chem Commun*. 2018;54(36):4613-4616.
96. Yang X, Wang Y, Tong X, Yang N. Strain engineering in electrocatalysts: fundamentals, progress, and perspectives. *Adv Energy Mater*. 2021;12(5):2102261.
97. Xie C, Yan D, Chen W, et al. Insight into the design of defect electrocatalysts: from electronic structure to adsorption energy. *Mater Today*. 2019;31:47-68.
98. Guo J, Zheng Y, Hu Z, et al. Direct seawater electrolysis by adjusting the local reaction environment of a catalyst. *Nat Energy*. 2023;8:264.
99. Wang X, Zhu Y, Vasileff A, et al. Strain effect in bimetallic electrocatalysts in the hydrogen evolution reaction. *ACS Energy Lett*. 2018;3(5):1198-1204.
100. Wang J, Han L, Huang B, Shao Q, Xin H, Huang X. Amorphization activated ruthenium-tellurium nanorods for efficient water splitting. *Nat Commun*. 2019;10(1):5692.
101. Tan H, Tang B, Lu Y, et al. Engineering a local acid-like environment in alkaline medium for efficient hydrogen evolution reaction. *Nat Commun*. 2022;13(1):2024.
102. Wen Q, Duan J, Wang W, et al. Engineering a local free water enriched microenvironment for surpassing platinum hydrogen evolution activity. *Angew Chem Int Ed*. 2022;61(35):e202206077.
103. Wen Q, Lin Y, Yang Y, et al. *In situ* chalcogen leaching manipulates reactant interface toward efficient amine electrooxidation. *ACS Nano*. 2022;16(6):9572-9582.
104. Hou L, Yang W, Li R, et al. Self-reconstruction strategy to synthesis of Ni/Co-OOH nanoflowers decorated with N, S co-doped carbon for high-performance energy storage. *Chem Eng J*. 2020;396:125323.
105. Liu X, Guo R, Huang W, Zhu J, Wen B, Mai L. Advances in understanding the electrocatalytic reconstruction chemistry of coordination compounds. *Small*. 2021;17(45):2100629.
106. Hou L, Yang W, Xu X, et al. In-situ activation endows the integrated Fe_3C/Fe@nitrogen-doped carbon hybrids with enhanced pseudocapacitance for electrochemical energy storage. *Chem Eng J*. 2019;375:122061.
107. Zhang C, Hou L, Yang W, et al. Phosphorization coupled electrochemical activation substantially enhances the energy storage performance of high mass loading nickel–cobalt-based materials. *Chem Eng J*. 2023;467:143410.

AUTHOR BIOGRAPHIES

Liqiang Hou received his Ph.D. from China University of Petroleum in 2021. He is an associate professor at Qingdao University of Science & Technology. His scientific interest includes the design and synthesis of electrocatalysts for HER and OER.

Jaephil Cho is a distinguished professor at UNIST (Republic of Korea). He is a director of the Battery R&D Center at UNIST. His current research is focused mainly on Li-ion, all-solid-state Li-ion, metal-air, and redox flow batteries for energy conversion and storage.

Xien Liu received his Ph.D. from Dalian University of Technology in 2006. He is a professor at Qingdao University of Science & Technology. His research interest is mainly focused on electrocatalysts for OER, ORR, HER, CO_2, and N_2 reduction.

How to cite this article: Hou L, Jang H, Gu X, et al. Design strategies of ruthenium-based materials toward alkaline hydrogen evolution reaction. *EcoEnergy*. 2023;1(1):16-44. https://doi.org/10.1002/ece2.4